This preprint has been submitted to *Science Advances* for peer-review on June 17th 2020.

The authors welcome any feedback and discussions.

Please contact us if you wish to discuss our manuscript:

pedroval07@gmail.com

Across-strike asymmetry of the Andes orogen linked to the age and geometry of the Nazca plate

Pedro Val[1,2*], *Jane K. Willenbring*[1]

[1] Scripps Institution of Oceanography, University of California San Diego, San Diego, CA.
[2] Now at Department of Geology, School of Mines, Federal University of Ouro Preto, Ouro Preto, MG, Brazil

*Correspondence to: pedroval07@gmail.com

One Sentence Summary: This study demonstrates that the position of the Andes mountains is largely a function of the Nazca plate's age and geometry and is inconsistent with the mechanism of orographic rainfall control on the distribution of exhumation within the orogen.

Abstract: The spine of Andes – the trace of the highest mountain topography – weaves back and forth, in places near the coastline, in others farther inland. Its position is thought to be partially influenced by the asymmetric distribution of rainfall causing the migration of the topographic divide (i.e. mountain peaks) in favor of the more erosive (wetter) side and consuming the less erosive (drier) side. Here, we demonstrate that erosion rates in the Andes are not controlled by rainfall and conclude that the position of this mountain chain is better described by the age and radius of curvature of the subducting Nazca plate. Our results suggest that mountain range migration might be a common component of orogenesis but for reasons different than those predicted by coupled climate-tectonic models. Cyclical variations in Andean orogeny might also accompany lateral migrations of mountain ranges.

Main Text:

Across-strike asymmetry of orogenic wedge topography forms by asymmetric mass fluxes through orogens. Climatically modulated erosion rates and tectonic controls on the spatial distribution of accretion and shortening form the two end-member controls on the orogenic asymmetry (Fig. 1). Orogenic asymmetries in the Andes mountains are thought to result from asymmetric erosion controlled by orographic precipitation (*1*) assuming zones of higher erosion rates coincide with higher, orographically-induced rainfall rates (*2*, *3*). These observations and interpretations are further supported by numerical models that successfully recreate orogenic wedge asymmetry due to climatically modulated erosion (*4*) (Fig. 1A). Furthermore, numerical models even predict that climatically modulated asymmetric mass fluxes can alter the strain distribution, thus feeding back into crustal deformation and overriding plate structure (*4*). The main caveat with all these arguments is in the difficulty to quantify how much of these relationships are a function of spatial coincidence between orographically enhanced rainfall or tectonically enhanced erosion rates (*5*, *6*).

Increasing evidence indicating that rainfall rates exert only secondary or minor controls on the erosive efficiency of mountains (*7–10*) suggest orogenic wedge asymmetry might not be rooted in climatically-controlled asymmetric erosion. If erosion and rainfall rates do not hold a cause-effect relationship, then models that use rainfall as a proxy for erosion may predict false patterns of mass flux. Indeed, both orogenic wedge (*11*) and cross-range mountain asymmetries (*12*) can be governed by the inclination of the tectonic uplift vector (i.e. pure vertical or angled) irrespective of rainfall distribution (Fig. 1B). Therefore, attributing orogen asymmetry to

orographic precipitation requires a correction for parameters that exert first order controls on tectonic uplift, but so far, this driver remains unexplored.

This work assesses whether the orographic precipitation and rain shadows in the Andes bear any relationship with observed orogenic wedge asymmetries. We quantify how much of the asymmetry in these wedges is attributed to tectonics versus orographic precipitation. Given the spatial correlation between rainfall rates and different topographic signatures (*1*), we demonstrate that landscapes might erode at similar paces but have different morphometries or vice-versa using compiled erosion rates (*13*). The results of this work provide empirical evidence that lateral mobility of mountain ranges through geologic time might be a common component of orogen evolution– independent of climate.

Wedge asymmetry controlled by subducting plate age and geometry

Slab geometry is strongly related to the rheology of the subducting plate and the interactions between overriding and subducting plates (*14*). The geometry is also directly linked to the deformation modes of the Andes (*15*) and to the age of the subducting Nazca slab, both of which are thought to strongly affect the distribution of deformation in the Andes orogen because of the changes in subducting plate thickness and buoyancy along strike (*16*, *17*). We used slab age (*18*) at the trench and slab geometry (equivalent radius of curvature, R_{pl} (*19*)) for the subducting Nazca slab to explore their potential controls on the asymmetry of the Andes orogen. Other radius of curvature estimates exist, but R_{pl} better describes complex slab geometries and bending dissipation (*19*) (Fig. 2, 3; Fig. S1). These metrics were correlated with measurements of

asymmetry of the Andes orogen in the same locations, which we calculated as the ratio of orthogonal distances between trench to peak mean topography and trench to back-arc deformation front adjusted to center symmetry at zero (see Fig. 1B; Fig. S2). Lastly, we collected data on the ratio of modern pro-wedge to retro-wedge 29-year average annual rainfall rates (*20*) to account for the role of orographic precipitation (Fig. S2). Where the retro-wedge rainfall rates are higher, we use the negative reciprocal of the ratio in order to preserve the same weight for all ratios (i.e. negative values for higher rainfall in the retro-wedge). While absolute rainfall rates were most likely different over the timescale of mountain building in the Andes, a 10-fold rainfall difference across trike is already expected for an Andes at 50% its modern height (*21*). The rainfall ratios we calculated therefore capture the orographic barriers over the timespan Andean orogenesis.

The position of magmatic arcs in several subduction zones worldwide is strongly related to the angle of the subducting slab (*22*). Our results demonstrate that this relationship remains a function of the subducting plate age and geometry even when corrected for the size of the orogenic wedge (Fig. 3A, B). Higher radii of curvature and younger slabs consistently lead to the mean topographic divides being farther from the trench and closer to the retro-arc deformation front (Fig. 3A, B). Outliers in the slab geometry to orogen asymmetry relationship remarkably coincide with the subduction of oceanic ridges and the Andean orocline (Fig. 2, 3B), which is unapparent in the relationship with slab age (Fig. 3A). This suggests that those key features of the Andean subduction zone might be the reason for the outliers in Figure 3B, although asymmetry estimates for latitudes 19°S and 21°S may be biased low due to the Altiplano Plateau (Fig. S2). Excluding the latter from our analysis does not affect our results (Fig. S3).

We also observe a relationship between rainfall ratio and orogen asymmetry that is weak when compared to slab age, yet statistically significant (Fig. 3C). To test the relative dependence of asymmetry on slab age and rainfall, we use an added variable analysis by adding slab age and rainfall ratio as independent predictors, one at a time in a multilinear model composed of the two. This analysis shows that the correlation is reduced to a small range in asymmetry after correcting for slab age (Fig. 3D), which is not the case after correcting for rainfall ratio (Fig. 3E). To test if rainfall ratio correlates with the orogen's deviation from symmetry, we invert the asymmetry metric (i.e. 1 – Wp/Wt), normalize it by 0.5 (maximum asymmetry), and take the absolute rainfall ratio for cases of higher rainfall in the retro-wedge, thus making both rainfall ratio and asymmetry metrics unidirectional. This shows no relationship between asymmetry and rainfall ratio (Fig. 3F), which is in line with the added variable analysis (Fig. 3E). The highest asymmetries are located where it rains two to three times on one said compared to the other, suggesting that the highest rainfall ratios observed for moderate asymmetries could be coincidental (Fig. 3C, F). Normalizing rainfall ratio by the height of mountains does not change these results, further supporting the latter statement (Fig. S4). Thus, orographic rainfall does not control the position of the mountain range divide despite being a consequence of it.

We maintain that just as the subducting plate age and geometry control mountain building, they also significantly control the asymmetry of orogenic wedges. Low-angle subduction increases plate coupling (*15*, *23*) and stress propagation into the overriding plate (*24*, *25*). Also, as slab angles decrease, the position of melting in the mantle wedge is pushed farther away from the trench and underneath the overriding arc (*22*). Consequently, slab angles also control the position

of magmatic production and therefore accretion to the orogen unlike collisional orogens. Moreover, the Nazca slab age and thickness in concert with the crustal thickness in the Andes have been used to explain the variations in shear force at the plate interface and ultimately the vertical and horizontal stress distributions in the Andes, with older slabs and thicker overriding plates associated with high vertical stresses near the trench (*16*), consistent with our results (Fig. 3A, B). By extension, this suggests that orographic precipitation cannot create asymmetric mass fluxes capable of offsetting the primary controls by subduction zone dynamics in the Andes, which is in line with previous studies (*9*) and is further explored in the next section.

Similar erosion rate but different landscape form

Rainfall can modulate the relationship between hillslope gradient and river channel steepness across different climatic regimes in the Andes (Fig. 4A-C). Our observations show that, for moderate hillslope gradients and high river steepnesses, basins in wetter parts of the Andes can have steeper hillslopes while the drier mountains have steeper rivers (Fig. 4A-C). These morphometric observations are in line with previous studies that revealed how Andean geomorphological domains can be distinguished as a function of regional climate (*1*, *26*). However, these distinctions need not require changes in erosion rates as these are most strongly controlled by hillslope gradients irrespective of rainfall rates (Fig. 4D-F). If anything, precipitation rates are important at the transition from arid to semi-arid climates, where a 250 mm/a rainfall-rate threshold might be enough to achieve high erosion rates (Fig. 4E, F). Further increases in rainfall rates are not associated with systematic changes in erosion rates (Fig. 4F) just as orogenic asymmetry is insensitive to high rainfall ratios (Fig. 3F). The variability in erosion rates decreases with increasing rainfall rates (Fig. 4E), consistent with observations in

the Andes and Himalaya (*27*, *28*). Similarly eroding landscapes have a wide range of river steepnesses, hillslope gradients, and rainfall rates but are much more dependent on hillslope gradient (Fig. 4D, E). These results are in line with global and regional studies (*2*, *7*, *9*, *10*, *13*)

That rainfall rates are imprinted in landscape form does not mean it can move mountains. Erosion rates on either side of a mountain range need to follow the rainfall trends for summits to systematically migrate laterally over the timescale of tectonic accretion. Such a pattern would require that hillslope transport and erosional efficiencies were controlled by rainfall as has been previously proposed (*29–31*). However, these predictions might be more complex due to the influence of vegetation for climates with greater than 250 mm/a rainfall rates (*28*). In the southern Central Andes, erosional efficiency in semi-arid landscapes is equivalent to that of temperate landscapes (*2*, *9*). Thus, assuming erosion rates are equivalent to rock uplift rates in our dataset, how landscapes respond to differences in tectonic regimes does not seem to be primarily a function of climate. This result is in line with the small or inexistent role of rainfall on orogen asymmetry (Fig. 3). These observations also reinforce previous notions from the literature that while rainfall modulates landscape form, it does not modulate the pace of erosion (*26*, *32*).

Lateral migration of mountain ranges

Our data suggests that the mountain range may change position within the orogenic wedge over time as a function of the subducting slab age and geometry. This result is a natural conclusion given the correlations we documented and inferences that the geometry of the subducting Nazca

plate changed systematically over at least the last 40 Ma (*33*). A change in the mountain range axis position does not require a change in the width of the orogenic wedge as has been demonstrated in numerical models (*34*) and agrees with observed variations of the loci of Andean mountain building in the northern Central Andes (*35*). In fact, it has been proposed that these relationships are all part of an Andean cycle of mountain building, magmatic production, and deformation (*36*, *37*).

Andean cyclicity has now been suggested based on geochemical (*36*), tectonic (*38*), and sedimentary (*39*) evidence. Not just shortening, but variations in accretionary fluxes, plate coupling and slab angle, and crustal root formation and foundering are all necessary components of this cycle (*35*, *36*, *39*) and are potentially part of the reason our results do not accompany the climate-induced wedge shape changes predicted by purely frictional wedges (*4*, *40*). This cyclicity is thought to govern the evolution of cordilleran orogeny over the western limits of the Americas from Patagonia to Alaska (*36*) with a recurrence time of 30 to 40 million years. This periodicity is strikingly matched by mantle subduction models (*34*), which in turn predict cyclicity in slab angles as a function of its depth and penetration into the lower mantle. Lastly, mantle flow in the wedge underneath the arc changes in concert with slab age, geometry, and the thickness of the Andes with direct consequences for the distribution of compressive forces orthogonally to the trench and into the Andes (*16*). Pairing our observations with the current understanding of the Andean orogeny evolution, we speculate that just as the magmatic arc changed over time, the position of the mountain range itself may have rocked back and forth solely as a function of the dynamics of the Andean subduction zone.

Figures

185

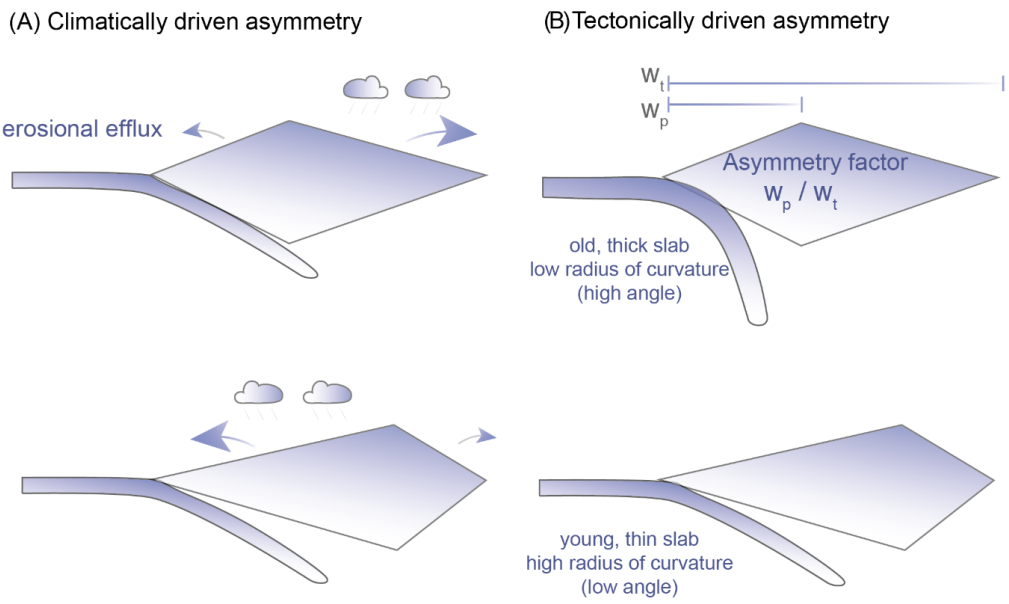

Fig. 1. Climate and tectonic end-member controls on orogenic wedge asymmetry. (A) Climatic control on orogenic asymmetry and (B) tectonic control on volcanic arc position based on the literature(4, 23). Arrows and their sizes in A indicate the volume of eroded material that is ultimately transported out of the orogenic wedge.

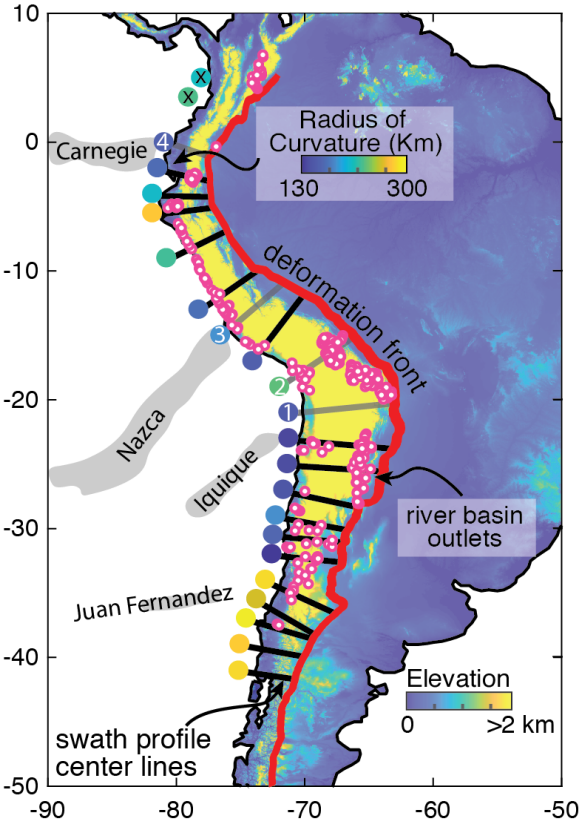

Fig. 2. Radius of curvature, elevation and location of swath profiles along the Andes. Colored circles show radius of curvature data(20) according to the top color scale and run along the Nazca trench. Red, bold line indicates the position of the deformation front. Pink circles are watershed outlets sampled for ^{10}Be-derived erosion rates. Black across-strike lines depict swaths used in the analysis of orogen asymmetry. Each swath profile is 100 km wide and goes from the trench out to the deformation front (solid red line). Two northernmost points (marked by "x") were excluded from geometry analyses as they might experience slab edge effects(50). Elevation of the Andes from 30 arc-second data colored according to the bottom color scale. Ridges on the Nazca plate (gray traces) coincide with outliers (faint numbered centerlines) in the asymmetry analysis (see Fig. 3): 1 - Orocline/Iquique ridge (-21°), 2 - Orocline (-19°), 3 - Nazca Ridge, 4 - Carnegie Ridge.

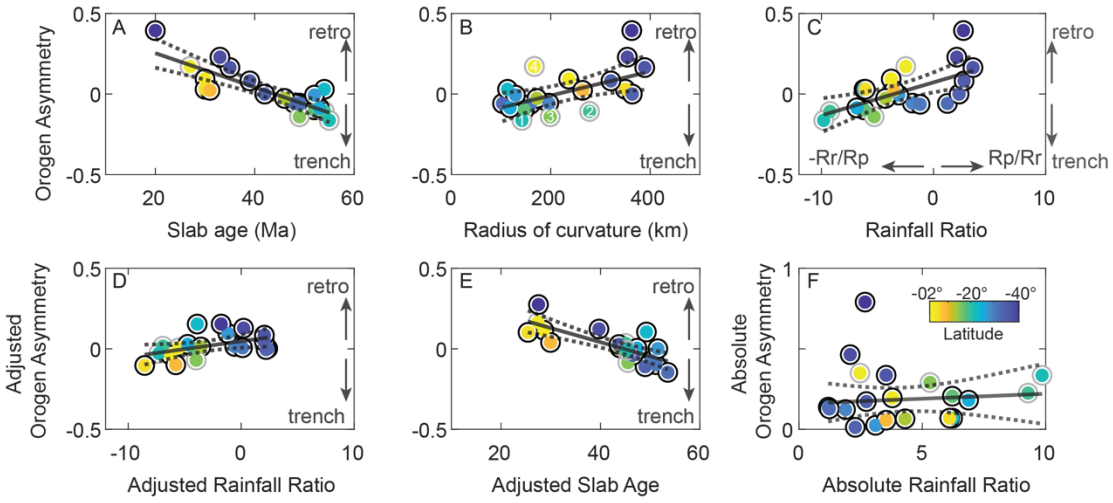

Fig. 3. Age and radius of curvature respectively explain 67% and 45% of the variance in orogenic asymmetry. Correlations between orogen asymmetry and (A) slab age at trench (R^2 = 0.67; p-value < 0.001; F-statistic = 37.3), (B) equivalent radius of curvature for a plastic plate (R^2 = 0.45; p-value < 0.01; F-statistic = 11.6), and (C) pro-wedge (Rp) to retro-wedge (Rr) rainfall ratio (R^2 = 0.45; p < 0.01; F-statistic = 11.5). Outliers (gray circles) non-coincidentally correspond to key features in the Nazca plate (shown in Figure 2) and were excluded from this regression but not from the others. (D) Added variable plot showing that accounting for slab age removes most of the variance in orogen asymmetry (R^2 = 0.19; p = 0.05; F-statistic = 4.3). (E) Added variable plot showing that accounting for rainfall ratio does not remove the variance in orogen asymmetry, which can still be accounted for using slab age (R^2 = 0.57; p < 0.01; F-statistic = 23.8). (F) Absolute rainfall ratios and orogen asymmetries normalized by 0.5 (0 is symmetric and 1 is 100% asymmetric) show no relationship with the absolute rainfall ratio (i.e. corrected for the expected direction of range migration) (R^2 = 0.04; p = 0.4; F-statistic = 0.7). The lower the F-statistic, the closer to the null-hypothesis that variables are uncorrelated. Based on these plots we interpret that asymmetric rainfall does not explain topographic asymmetry in the Andes. The viscous plate equivalent radius of curvature, $R_{vs}(20)$, yields similar results as the one in Fig. 3B while a minimum radius of curvature used for simple slab geometries, $R_{min}(20)$, does not (Fig. S1). All regressions were performed using the Matlab's fitlm function with the robust routine which minimizes the effects of outliers. The same analysis using mean centered data is presented in the Supplementary Figure S5 along with regression coefficients for slope comparison (Supplementary Table S1).

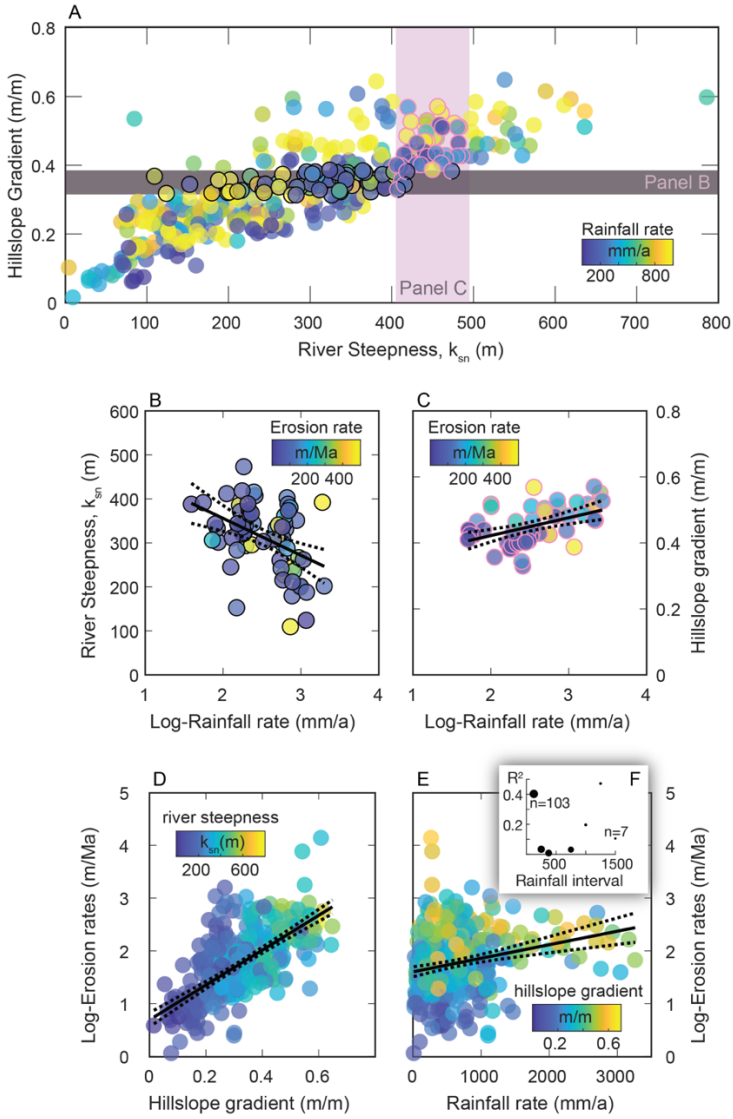

Fig. 4. Wetter landscapes have steeper hillslopes while dryer landscapes have steeper rivers, but different morphometries have similar erosion rates independently of rainfall. Shown are relationships extracted from 377 basin-wide erosion rate data points in the Andes. Panel A shows relationships between hillslope gradient and river steepness colored by rainfall rates, with shaded bands indicating subsampled examples, B and C. For given hillslope gradient (B) and river steepness (C) classes (bands in panel A), increases in rainfall are associated with shallower rivers (B, $R^2 = 0.19$; $p < 0.01$; F-statistic = 14) and steeper hillslopes (C, $R^2 = 0.24$; $p < 0.01$; F-statistic = 16). Erosion rates are more strongly controlled by hillslope gradients (D, $R^2 = 0.44$; $p < 0.01$; F-statistic = 291) than by rainfall rates (E, $R^2 = 0.06$; $p < 0.01$; F-statistic = 23). Erosion rate variability decreases with increasing rainfall (E). Rainfall rates are well correlated with erosion rates in arid to semiarid (0 – 250 mm/a) landscapes as indicated by an R^2 of ~0.4 but these metrics are poorly correlated in wetter landscapes (F). R^2 values were computed in intervals of

250 mm/a up to 1000 mm/a, and in intervals of 500 mm/a up to 3000 mm/a rainfall rates. The size of the marker indicates the number of data points in each rainfall bin. Rainfall rate and erosion rate data obtained from the literature(14, 21).

235

References:

1. D. R. Montgomery, G. Balco, S. D. Willett, Climate, tectonics, and the morphology of the Andes. *Geology*. **29**, 579 (2001).

2. S. Carretier, V. Regard, R. Vassallo, G. Aguilar, J. Martinod, R. Riquelme, E. Pepin, R. Charrier, G. Hérail, M. Farías, J.-L. Guyot, G. Vargas, C. Lagane, Slope and climate variability control of erosion in the Andes of central Chile. *Geology*. **41**, 195–198 (2013).

3. B. Bookhagen, M. R. Strecker, Spatiotemporal trends in erosion rates across a pronounced rainfall gradient: Examples from the southern Central Andes. *Earth Planet. Sci. Lett.* **327**–**328**, 97–110 (2012).

4. S. D. Willett, Orogeny and orography: The effects of erosion on the structure of mountain belts. *J. Geophys. Res.* **104**, 28957–28981 (1999).

5. M. R. Strecker, R. Alonso, B. Bookhagen, B. Carrapa, I. Coutand, M. P. Hain, G. E. Hilley, E. Mortimer, L. Schoenbohm, E. R. Sobel, Does the topographic distribution of the central Andean Puna Plateau result from climatic or geodynamic processes? *Geology*. **37**, 643–646 (2009).

6. M. R. Strecker, R. N. Alonso, B. Bookhagen, B. Carrapa, G. E. Hilley, E. R. Sobel, M. H. Trauth, Tectonics and Climate of the Southern Central Andes. *Annu. Rev. Earth Planet. Sci.* **35**, 747–787 (2007).

7. M. A. Harel, S. M. Mudd, M. Attal, Global analysis of the stream power law parameters based on worldwide ^{10}Be denudation rates. *Geomorphology*. **268**, 184–196 (2016).

8. V. Godard, D. L. Bourlès, F. Spinabella, D. W. Burbank, B. Bookhagen, G. B. Fisher, A. Moulin, L. Léanni, Dominance of tectonics over climate in himalayan denudation.

Geology. **42**, 243–246 (2014).

9. P. Val, A. L. Venerdini, W. Ouimet, P. Alvarado, G. D. Hoke, Tectonic control of erosion in the southern Central Andes. *Earth Planet. Sci. Lett.* **482**, 160–170 (2018).

10. E. W. Portenga, P. R. Bierman, Understanding Earth's eroding surface with ^{10}Be. *GSA Today*. **21**, 4–10 (2011).

11. S. D. Willett, R. Slingerland, N. Hovius, Uplift, Shortening, and Steady State Topography in Active Mountain Belts. *Am. J. Sci.* **301**, 455–485 (2001).

12. S. R. Miller, R. L. Slingerland, E. Kirby, Characteristics of steady state fluvial topography above fault-bend folds. *J. Geophys. Res.* **112**, F04004 (2007).

13. A. T. Codilean, H. Munack, T. J. Cohen, W. M. Saktura, A. Gray, S. M. Mudd, OCTOPUS: An open cosmogenic isotope and luminescence database. *Earth Syst. Sci. Data*. **10**, 2123–2139 (2018).

14. A. F. Holt, B. A. Buffett, T. W. Becker, Overriding plate thickness control on subducting plate curvature. *Geophys. Res. Lett.* **42**, 3802–3810 (2015).

15. B. K. Horton, Tectonic regimes of the Central and Southern Andes: Response to variations in plate coupling during subduction. *Tectonics*. **37**, 1–28 (2018).

16. F. A. Capitanio, C. Faccenna, S. Zlotnik, D. R. Stegman, Subduction dynamics and the origin of Andean orogeny and the Bolivian orocline. *Nature*. **480**, 83–86 (2011).

17. P. Molnar, T. Atwater, Interarc spreading and Cordilleran tectonics as alternates related to the age of subducted oceanic lithosphere. *Earth Planet. Sci. Lett.* **41**, 330–340 (1978).

18. S. Lallemand, A. Heuret, D. Boutelier, On the relationships between slab dip, back-arc

stress, upper plate absolute motion, and crustal nature in subduction zones. *Geochemistry, Geophys. Geosystems*. **6** (2005), doi:10.1029/2005GC000917.

19. B. A. Buffett, A. Heuret, Curvature of subducted lithosphere from earthquake locations in the Wadati-Benioff zone. *Geochemistry, Geophys. Geosystems*. **12**, 1–13 (2011).

20. M. New, D. Lister, M. Hulme, I. Makin, A high-resolution data set of surface climate over global land areas. *Clim. Res.* **21**, 1–25 (2002).

21. N. Insel, C. J. Poulsen, T. A. Ehlers, C. Sturm, Response of meteoric δ 18O to surface uplift - Implications for Cenozoic Andean Plateau growth. *Earth Planet. Sci. Lett.* **317**–**318**, 262–272 (2012).

22. T. L. Grove, C. B. Till, E. Lev, N. Chatterjee, E. Médard, Kinematic variables and water transport control the formation and location of arc volcanoes. *Nature*. **459**, 694–697 (2009).

23. Q. Bletery, A. M. Thomas, A. W. Rempel, L. Karlstrom, A. Sladen, L. de Barros, Mega-earthquakes rupture flat megatrhusts. *Science (80-.).* **354** (2016), doi:10.1126/science.aag0482.

24. A. Heuret, C. P. Conrad, F. Funiciello, S. Lallemand, L. Sandri, Relation between subduction megathrust earthquakes, trench sediment thickness and upper plate strain. *Geophys. Res. Lett.* **39** (2012), doi:10.1029/2011GL050712.

25. W. P. Schellart, Overriding plate shortening and extension above subduction zones: A parametric study to explain formation of the Andes Mountains. *Bull. Geol. Soc. Am.* **120**, 1441–1454 (2008).

26. N. M. Gasparini, K. X. Whipple, Diagnosing climatic and tectonic controls on

topography: Eastern flank of the northern Bolivian Andes. *Lithosphere* (2014), doi:10.1130/L322.1.

27. S. M. Olen, B. Bookhagen, M. R. Strecker, Role of climate and vegetation density in modulating denudation rates in the Himalaya. *Earth Planet. Sci. Lett.* **445**, 57–67 (2016).

28. J. Starke, T. A. Ehlers, M. Schaller, Latitudinal effect of vegetation on erosion rates identified along western South America. *Science (80-.).* **367**, 1358–1361 (2020).

29. J. L. Dixon, A. M. Heimsath, J. Kaste, R. Amundson, Climate-driven processes of hillslope weathering. *Geology*. **37**, 975–978 (2009).

30. K. L. Ferrier, K. L. Huppert, T. Perron, Climatic control of bedrock river incision. *Nature*. **496**, 206–211 (2013).

31. P. W. Richardson, J. T. Perron, N. D. Schurr, Influences of climate and life on hillslope sediment transport. *Geology*. **47**, 423–426 (2019).

32. E. B. Safran, P. R. Bierman, R. Aalto, T. Dunne, K. X. Whipple, M. Caffee, Erosion rates driven by channel network incision in the Bolivian Andes. *Earth Surf. Process. Landforms*. **30**, 1007–1024 (2005).

33. V. A. Ramos, A. Folguera, Andean flat-slab subduction through time. *Geol. Soc. London, Spec. Publ.* **327**, 31–54 (2009).

34. W. P. Schellart, Andean mountain building and magmatic arc migration driven by subduction-induced whole mantle flow. *Nat. Commun.* **8**, 1–13 (2010).

35. C. N. Garzione, N. McQuarrie, N. D. Perez, T. A. Ehlers, S. L. Beck, N. Kar, N. Eichelberger, A. D. Chapman, K. M. Ward, M. N. Ducea, R. O. Lease, C. J. Poulsen, L. S. Wagner, J. E. Saylor, G. Zandt, B. K. Horton, Tectonic Evolution of the Central Andean

Plateau and Implications for the Growth of Plateaus. *Annu. Rev. Earth Planet. Sci.* **45**, 529–559 (2017).

36. P. G. DeCelles, M. N. Ducea, P. Kapp, G. Zandt, Cyclicity in Cordilleran orogenic systems. *Nat. Geosci.* **2**, 251–257 (2009).

37. V. Ramos, Anatomy and global context of the Andes: main geologic features and the Andean orogenic cycle. *Geol. Soc. Am. Mem.* **204**, 31–65 (2009).

38. R. B. Anderson, S. P. Long, B. K. Horton, S. N. Thomson, A. Z. Calle, D. F. Stockli, Orogenic Wedge Evolution of the Central Andes, Bolivia (21°S): Implications for Cordilleran Cyclicity. *Tectonics*. **37**, 3577–3609 (2018).

39. B. K. Horton, F. Fuentes, Sedimentary record of plate coupling and decoupling during growth of the Andes. *Geology*. **44**, 647–650 (2016).

40. K. X. Whipple, The influence of climate on the tectonic evolution of mountain belts. *Nat. Geosci.* **2**, 97–104 (2009).

41. W. Schwanghart, D. Scherler, Short Communication: TopoToolbox 2 – MATLAB-based software for topographic analysis and modeling in Earth surface sciences. *Earth Surf. Dyn.* **2**, 1–7 (2014).

42. B. Bookhagen, M. R. Strecker, Orographic barriers, high-resolution TRMM rainfall, and relief variations along the eastern Andes. *Geophys. Res. Lett.* **35**, L06403 (2008).

43. J. O. Stone, *J. Geophys. Res.*, in press.

44. F. Kober, G. Zeilinger, K. Hippe, O. Marc, T. Lendzioch, R. Grischott, M. Christl, P. W. Kubik, R. Zola, Tectonic and lithological controls on denudation rates in the central Bolivian Andes. *Tectonophysics*. **657**, 230–244 (2015).

45. R. A. Dibiase, Short communication : Increasing vertical attenuation length of cosmogenic nuclide production on steep slopes negates topographic shielding corrections for catchment erosion rates, 923–931 (2018).

46. NASA Shuttle Radar Topography Mission (SRTM)(2013). Shuttle Radar Topography Mission (SRTM) Global. Distributed by OpenTopography. Accessed: 2020-05-03, doi:10.5069/G9445JDF.

47. A. M. Forte, K. X. Whipple, Short communication: The Topographic Analysis Kit (TAK) for TopoToolbox. *Earth Surf. Dyn.* **7**, 87–95 (2019).

Acknowledgments: P.V. was funded by the US National Science Foundation (Award #1651243 to JKW) and CAPES – Coordenação de Aperfeiçoamento de Pessoal de Nível Superior (#0515-12-4); **Author contributions:** PV: Data acquisition and Compilation, Data analysis, Original draft preparation; PV and JKW: Conceptualization, Methodology, Writing, Reviewing, and Editing; **Competing interests:** Authors declare no competing interests; **Data and materials availability:** All data is available in the supplementary materials.

Supplementary Materials:

Materials and Methods
Figures S1-S5
Table S1
External Databases S1-S3
References (*41-47*)

Supplementary Materials for

Across-strike asymmetry of the Andes orogen linked to the age and geometry of the Nazca plate

P. Val[1,2], J.K. Willenbring[1]*

Correspondence to: pedroval07@gmail.com

This PDF file includes:

Materials and Methods
Figs. S1 to S5
Table S1
Captions for Data S1 to S3

Other Supplementary Materials for this manuscript include the following:

Data Table S1 to S3

Data Table S1: Orogen data: Radius of curvature, slab age, asymmetry, and precipitation ratio.

Data Table S2: Erosion rate and topographic data.

Data Table S3: Excluded erosion rate data.

Materials and Methods

Orogen asymmetry, slab age and radius of curvature, and rainfall ratio

Orogenic asymmetries were calculated as the ratio of distances between trench to peak mean topography and trench to retro arc deformation front (based on the published maps (*15*, *37*)), thus ranging from 0 to 1, the latter being close to the retro arc deformation front (Fig. S2). We acknowledge that the pro arc deformation fronts sometimes are not directly on the trench but somewhere between the trench and prowedge; however, the location of this prowedge front is not always well defined, unlike the trench. Furthermore, the subduction zone interface is where the ultimate megathrust is located and defines the western limit of the Andes orogen (*37*).

We chose the peak mean topography as an approximation of the greatest mass within the mountain range. Peak mean topography was identified in 100 km wide swath topographic profiles computed using Topotoolbox (*41*). A gaussian curve was fit to the mean topography, after which a tallest point was identified. Swath center lines follow the trench-normal azimuths (*19*) starting at the Nazca trench outline (Supplementary Dataset). Radius of curvature (*19*) and slab age (*18*) at the starting point of the swath centerlines were comparted to the orogen asymmetry measurements. Data are provided in the Supplementary Dataset.

Rainfall ratio is calculated as the ratio between prowedge and retrowedge average rainfall. To do this, we averaged the rainfall rates west of the peak mean topography and divided those by the average east of it. We used the 29-year average rainfall rates from the global dataset reanalyzed by the Climate Research Unit (*20*) and extends south of 35°S, unlike TRMM 2b31 (*42*). Rainfall ratios greater than one denote orographic effects with greater rainfall in the pro-wedge side. Ratios smaller than one were inverted and multiplied by -1 to preserve the scale of rainfall ratio on both sides. These ratios were then compared to the orogen asymmetry metric.

Morphometric indices and erosion rates

Erosion rates and basin morphometrics were paired in order to compare landscape morphometry and erosion rates (see Supplementary Dataset). The latter was obtained from the Octopus 2018 database (*13*). The entire Andean database contains 477 basins and we added 9 more from the Southern Central Andes yet not included to the dataset (*9*) for a total of 486 basins. Erosion rates from the latter were recalculated to the same production rate scaling method (*43*) used in the Octopus database. We excluded 65 replicates but do not have information on grain sizes, so those were not distinguished in the dataset. We also removed basins with drainage areas greater than 10^4 km^2 (39 basins) as these contain large alluvial areas and do not drain predominantly one uplifting block. This way, all of the included basins have outlets west of the Andean deformation front (Fig. 2). One basin from ~49°S Latitude was excluded as its morphometry would not be comparable to the rest of the dataset given glacial activity. Lastly, we excluded 9 basins from the Bolivian Sub-Andean thrust fronts as these thrusts uplift exceptionally erodible sedimentary rocks that produce high erosion rates that are outliers in the original dataset (*44*). All of the data, including excluded ones, are provided in Supplementary Dataset. It is worth noting that this dataset uses topographic shielding calculations which can bias erosion rates low (*45*) in the steepest basins. Therefore, not accounting for topographic shielding would potentially increase the dependence of erosion rates on hillslope gradient shown in Fig. 4D. For more information on cosmogenic nuclides and erosion rate calculations, see Codilean et al (*13*).

For the same basins, we extracted morphometric data from Shuttle Radar Topographic Mission (SRTM) 90 m dataset (*46*) using Topotoolbox (*41*) and the Topographic Analysis Kit (*47*) with default settings. We used 30 m SRTM data (*46*) for basins with drainage area smaller than 5 square kilometers. In the former, basin morphometrics were calculated using a threshold drainage area of 10^6 m^2 and in the latter, 5 x 10^5 m^2. Both hillslope gradient and river steepness data are basin-wide averages. Hillslope gradient was first calculated as the steepest slope (m/m) in an eight-cell neighborhood around each pixel and then averaged over the area of the analyzed basins. River steepness (k_{sn}) is first calculated for distinct river stretches using a concavity index of 0.5 for all rivers with drainage area greater than the threshold area (quick method in TAK (*47*)). Basin-wide rainfall rates were obtained from the 11-year average Topographic Rainfall Measurement Mission 2b31 dataset (*42*), which is the most widely used in basin-wide erosion rate analyses.

Supplementary Figures

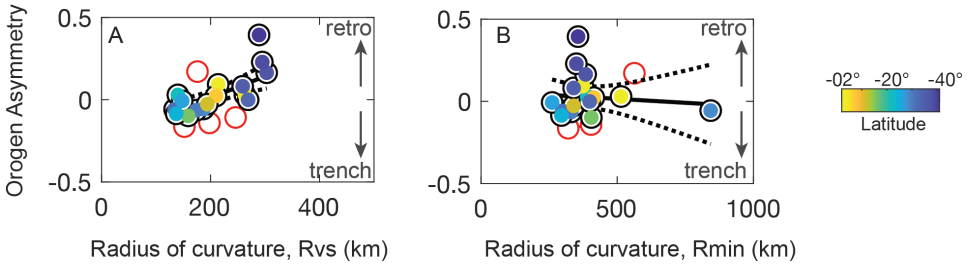

Fig S1: Other estimates of radius of curvature and their relationship with orogen asymmetry. Same panel as Figure 3B in the main text but for the equivalent radius of curvature R_{vs} for a viscous plate (A) and minimum radius of curvature Rmin (B) from Buffett and Heuret (2011) (*19*). Red circles are outliers identified in Figure 2 and 3 in the main text.

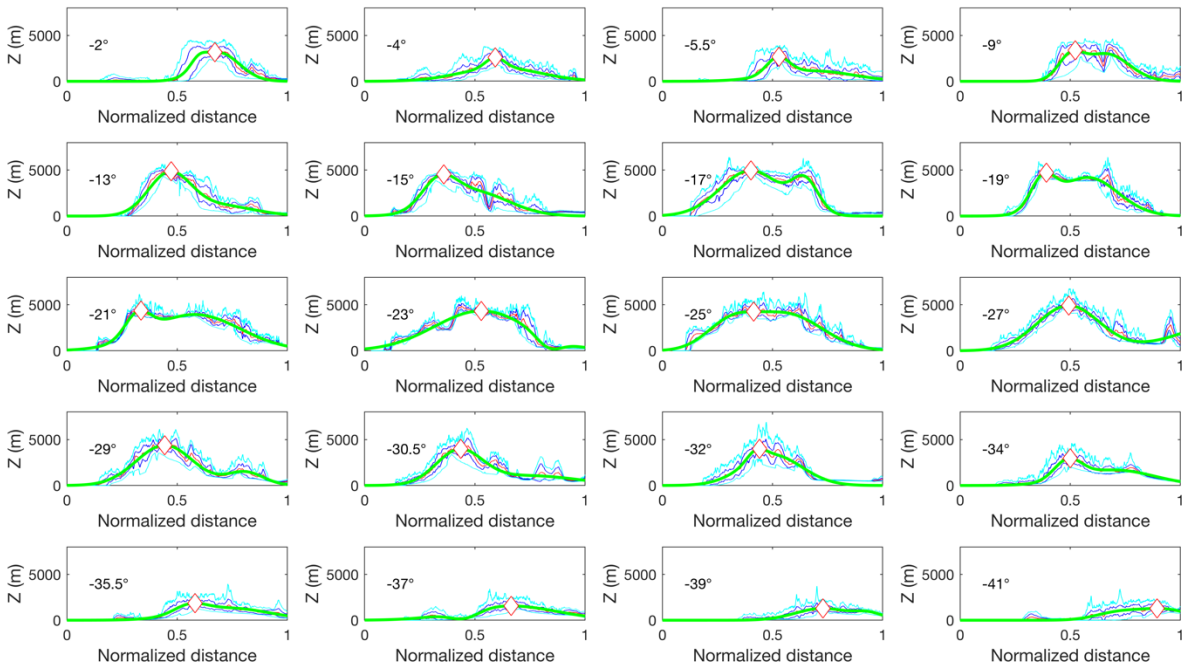

Fig S2: Swath profiles and estimated asymmetry factor per swath. The panels show the topographic swath profiles across the Andes orogen for the locations shown in the main paper. The figures depict mean (red line), minimum (lower cyan line), maximum (upper cyan line) and standard deviation (blue lines) for elevations along a 100 km wide swath about a centerline (red line in map immediately below each swath). A gaussian fit to the average elevation to smooth out noises along the profile is shown in green along which the highest altitude is marked by a red diamond. The position of the diamond informs the asymmetry of the orogen.

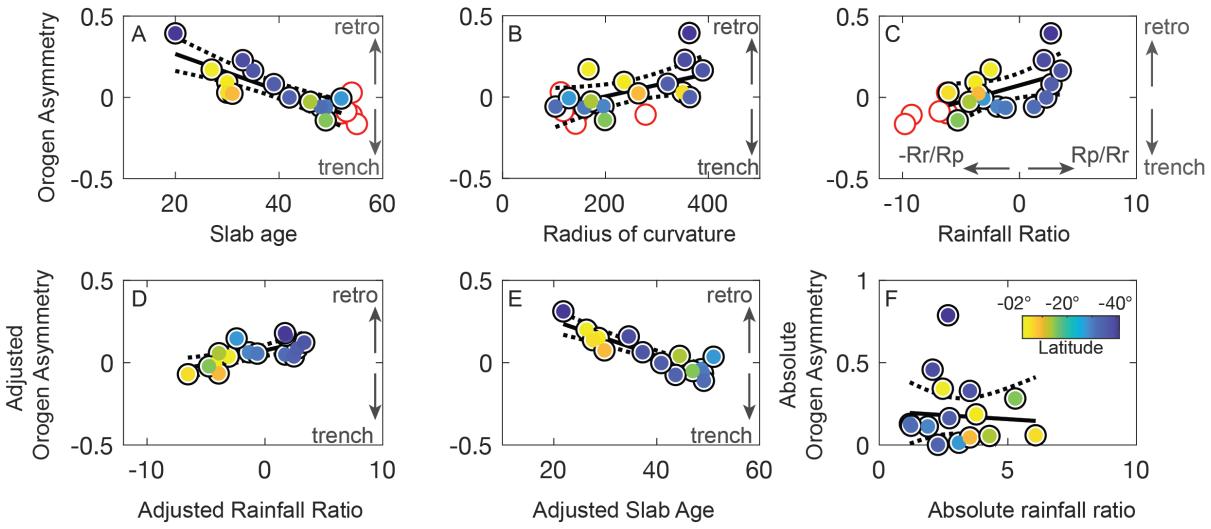

Fig S3: Excluding the Altiplano plateau does not affect our results and improves partial regressions with slab age. Here, we excluded data from latitudes -17° through -25°. Red data points in panels A through C denote excluded data. (A) $R^2 = 0.65$; p-value < 0.001; F-statistic = 24.5, (B) $R^2 = 0.29$; p-value < 0.05; F-statistic = 5.17, (C) $R^2 = 0.22$; p-value < 0.1; F-statistic = 3.71, (D) $R^2 = 0.46$; p-value < 0.01; F-statistic = 10.9, (E) $R^2 = 0.77$; p-value < 0.001; F-statistic = 43.5, (F) $R^2 = 0.03$; p-value = 0.5; F-statistic = 0.4.

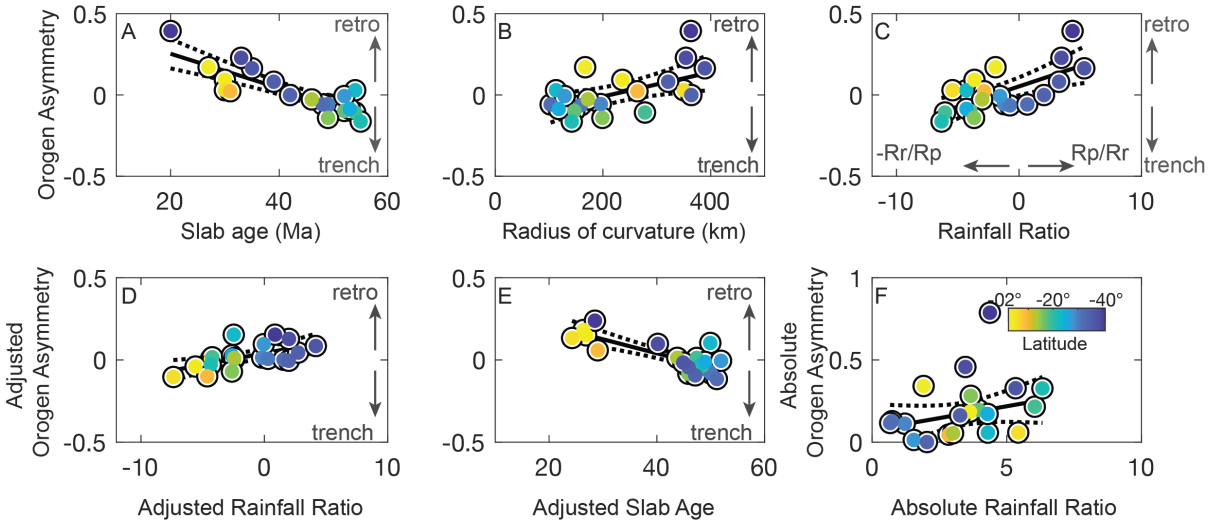

Fig S4: Normalizing rainfall ratios by maximum elevation does not affect our results. Here, rainfall ratio data were normalized by the maximum elevation (scaled 0 to 1, the latter being the maximum in the dataset) in the swath profile and subsequently multiplied by 0.5 to reduce spread in the data. This slightly improves the relationship in Panel C but does not remove the dominance of slab age over the regression. (A) $R^2 = 0.67$; p-value < 0.001; F-statistic = 37.3, (B) $R^2 = 0.31$; p-value < 0.02; F-statistic = 7.92, (C) $R^2 = 0.42$; p-value < 0.005; F-statistic = 12.9, (D) $R^2 = 0.35$; p-value < 0.01; F-statistic = 9.56, (E) $R^2 = 0.66$; p-value < 0.001; F-statistic = 34.3, (F) $R^2 = 0.14$; p-value = 0.1; F-statistic = 2.95.

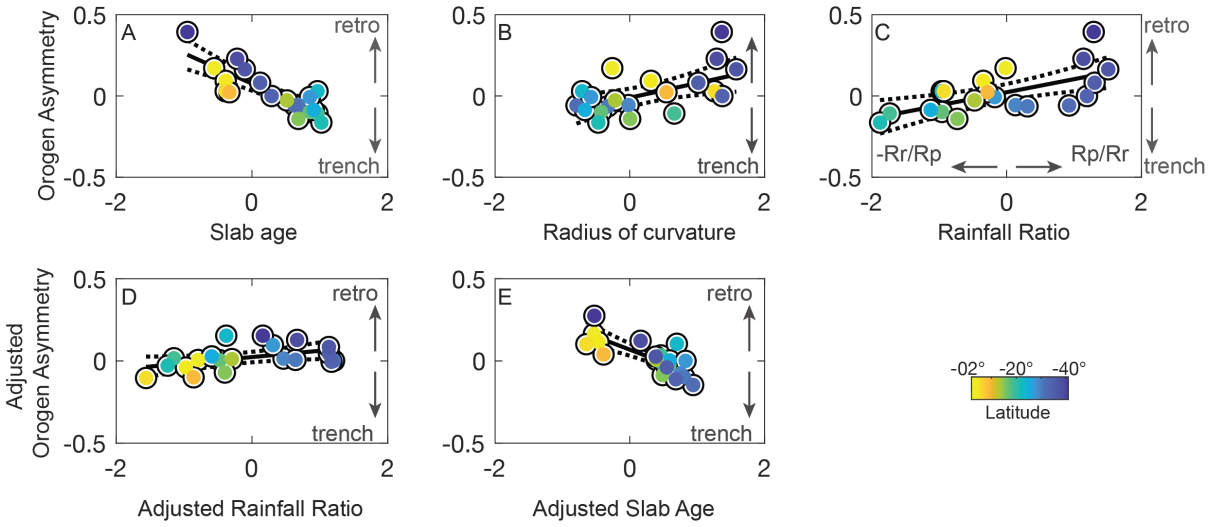

Fig S5: Mean-centered regression analyses show higher slope dependence of orogen asymmetry on tectonic metrics. Here we performed the same analysis as in Figure 3 of the main text but independent variables (slab age, radius of curvature, rainfall ratio) had the mean value subtracted and normalized by the standard deviation. Regression statistics and coefficients are presented in the Supplementary Table S1.

Supplementary Tables

Table S1: Summary statistics of mean-centered regressions to the data presented in Fig S5 and Fig. 3 (not centered).

	Regression coefficients				Regression performance			
	Estimate	Standard Error	t-statistic[a]	p-value for t-statistic[b]	RMSE	R^2	F-statistic[c]	p-value
Slab age								
Intercept	0.0755	0.0206	3.6582	0.0018	0.0818	0.674	37.3	9.12E-06
Slope	-0.1873	0.0307	-6.1013	0.0000				
Radius of curvature [d]								
Intercept	-0.0018	0.0225	-0.0797	0.9376	0.0843	0.453	11.6	0.00429
Slope	0.0820	0.0248	3.3118	0.0051				
Rainfall ratio								
Intercept	0.0229	0.0243	0.9409	0.3592	0.108	0.389	11.5	0.00329
Slope	0.0806	0.0238	3.3811	0.0033				
Partial regression (adjusted to slab age)								
Intercept	0.0194	0.0161	1.1993	0.2460	0.0718	0.191	4.26	0.0537
Slope	0.0379	0.0185	2.0467	0.0556				
Partial regression (adjusted to rainfall ratio)								
Intercept	0.0631	0.0188	3.3570	0.0035	0.0716	0.57	23.8	0.00012
Slope	-0.1537	0.0316	-4.8700	0.0001				

a. Estimate / Standard Error. The t-statistic provides a score of how the estimate differs from the null hypothesis that the estimate is zero.
b. Significance of the t-statistic. A value <0.05, for example, is significant at the 5% level.
c. Score showing how the model performs against a model with constant terms.
d. Regression excludes outliers 1-4 as outlined in the main text

Data Table S1. (separate file)
Data Table S1: Orogen data: Radius of curvature, slab age, asymmetry, and precipitation ratio.

Data Table S2. (separate file)
Data Table S2: Erosion rate and topographic data.

Data Table S3. (separate file)
Data Table S3: Excluded erosion rate data.

Data Table S1: Orogen data: Radius of curvature, slab age, asymmetry, and precipitation ratio.

Lat	Long	Az	Slab Age	Rmin	Rvs	Rpl	Asymmetry[a]	Rainfall ratio[b]
-2,00	-81,50	102,00	27,00	563,00	176,00	167,00	0,17	-2,47
-4,00	-81,90	91,00	30,00	374,00	214,00	236,00	0,09	-3,77
-5,50	-81,90	82,90	30,00	514,00	263,00	350,00	0,03	-6,08
-9,00	-80,80	64,00	31,00	414,00	210,00	264,00	0,02	-3,52
-13,00	-78,30	55,50	46,00	340,00	194,00	172,00	-0,03	-4,28
-15,00	-76,60	50,00	49,00	404,00	198,00	199,00	-0,14	-5,29
-17,00	-74,10	37,80	52,00	405,00	159,00	147,00	-0,10	-6,18
-19,00	-72,00	56,40	54,00	337,00	246,00	278,00	-0,11	-9,23
-21,00	-71,30	84,40	55,00	320,00	152,00	142,00	-0,16	-9,80
-23,00	-71,30	94,70	54,00	390,00	140,00	113,00	0,03	-6,20
-25,00	-71,40	93,30	53,00	295,00	137,00	118,00	-0,09	-6,84
-27,00	-71,70	101,10	52,00	261,00	148,00	129,00	-0,01	-3,10
-29,00	-72,30	99,40	49,00	843,00	187,00	196,00	-0,06	-1,89
-30,50	-72,50	94,30	49,00	331,00	174,00	159,00	-0,06	-1,19
-32,00	-72,60	94,80	48,00	298,00	134,00	103,00	-0,06	1,24
-34,00	-73,10	113,30	42,00	399,00	269,00	364,00	0,00	2,28
-35,50	-73,80	118,40	39,00	340,00	259,00	321,00	0,08	2,73
-37,00	-74,60	105,00	35,00	384,00	303,00	389,00	0,16	3,52
-39,00	-75,10	99,00	33,00	350,00	295,00	354,00	0,23	2,08
-41,00	-75,30	97,00	20,00	356,00	289,00	363,00	0,39	2,67

a. Asymmetry is calculated as (Wp/Wt - 0.5)

b. Positive values are Pro/Retro wedge rainfall ratio. Negative values are -Retro/Pro wedge rainfall ratio.

Dataset for Val and Willenbring (not peer reviewed)

Data Table S2: Erosion rate and topographic data.

Octopus Erosion Rate Dataset				
Octopus Flag	**X_WGS84**	**Y_WGS84**	**EBE_MMKYR**	**EBE_ERR**
	°Lon	°Lat	(or m/Ma)	1s
'S025WTS011'	-68,28	-15,30	185,72	34,83
'S025WTS012'	-68,24	-15,31	166,79	33,39
'S025WTS013'	-68,21	-15,31	205,97	39,07
'S025WTS014'	-68,17	-15,41	67,02	14,59
'S025WTS015'	-68,15	-15,39	164,40	35,86
'S025WTS017'	-67,88	-15,50	282,60	54,22
'S025WTS018'	-67,87	-15,51	435,24	86,26
'S025WTS019'	-67,84	-15,51	156,10	32,26
'S025WTS001'	-68,64	-15,79	776,81	146,92
'S025WTS020'	-67,67	-15,76	333,65	68,62
'S025WTS021'	-67,58	-15,98	39,42	8,31
'S025WTS022'	-67,59	-16,00	225,63	49,05
'S025WTS023'	-67,63	-16,04	143,12	30,08
'S025WTS024'	-67,65	-16,28	208,61	42,34
'S025WTS025'	-68,12	-16,14	415,27	76,92
'S025WTS026'	-68,07	-16,11	505,89	94,74
'S025WTS027'	-68,04	-16,08	390,13	76,92
'S025WTS028'	-68,00	-16,05	349,85	65,61
'S025WTS029'	-67,97	-16,88	192,66	36,08
'S025WTS002'	-68,64	-15,78	309,36	61,08
'S025WTS030'	-67,69	-16,94	175,93	32,34
'S025WTS031'	-67,20	-16,81	170,01	34,18
'S025WTS032'	-67,21	-16,77	299,80	61,14
'S025WTS033'	-67,22	-16,76	161,36	31,89
'S025WTS003'	-68,65	-15,76	565,02	116,15
'S025WTS041'	-67,34	-16,51	338,45	64,43
'S025WTS042'	-67,30	-16,48	385,68	72,71
'S025WTS044'	-67,47	-16,43	107,11	21,62

'S025WTS045'	-67,48	-16,42	235,09	47,29
'S025WTS046'	-67,43	-16,32	817,13	164,42
'S025WTS048'	-67,43	-16,32	222,14	45,21
'S025WTS049'	-67,61	-16,39	434,39	83,01
'S025WTS004'	-68,67	-15,71	639,09	126,87
'S025WTS050'	-67,64	-16,40	566,36	113,19
'S025WTS051'	-67,81	-16,36	337,66	67,87
'S025WTS054'	-67,91	-16,31	482,89	89,68
'S025WTS055'	-67,89	-16,31	291,52	53,85
'S025WTS005'	-68,68	-15,67	191,76	36,57
'S025WTS006'	-68,48	-15,33	197,29	36,82
'S025WTS007'	-68,60	-15,46	202,01	37,59
'S025WTS008'	-68,54	-15,41	290,27	60,19
'S035WTS010'	-78,89	-2,88	36,28	7,24
'S035WTS012'	-78,89	-2,91	67,32	13,94
'S035WTS013'	-78,93	-2,77	72,63	14,11
'S035WTS003'	-78,90	-2,96	19,54	3,75
'S035WTS004'	-78,91	-2,94	43,21	8,59
'S035WTS007'	-78,95	-3,04	21,04	4,05
'S035WTS008'	-78,93	-2,94	37,08	7,43
'S035WTS009'	-78,92	-2,97	54,15	10,85
'S048WTS001'	-69,88	-18,35	23,19	4,41
'S048WTS002'	-70,02	-18,40	22,83	4,29
'S048WTS003'	-70,30	-18,40	23,80	4,63
'S048WTS004'	-69,63	-18,00	10,95	2,48
'S048WTS005'	-69,65	-18,10	11,39	2,22
'S059WTS010'	-79,91	-5,14	125,26	26,88
'S059WTS011'	-80,02	-5,21	31,54	7,58
'S059WTS012'	-80,29	-4,98	52,06	13,77
'S059WTS013'	-80,38	-4,93	12,85	3,56
'S059WTS014'	-80,65	-5,24	18,31	4,52
'S059WTS019'	-80,05	-5,02	89,39	22,31
'S059WTS023'	-79,88	-5,06	101,01	21,37

'S059WTS002'	-80,01	-4,96	108,87	23,16
'S059WTS003'	-80,06	-5,03	107,17	23,64
'S059WTS004'	-80,13	-5,09	100,49	22,84
'S059WTS005'	-80,16	-5,10	73,71	16,82
'S059WTS006'	-79,83	-5,03	28,00	6,45
'S059WTS007'	-79,85	-5,05	141,71	37,03
'S059WTS008'	-79,87	-5,06	211,01	48,89
'S059WTS009'	-79,90	-5,11	100,36	27,04
'S061WTS010'	-64,08	-19,61	144,52	27,83
'S061WTS013'	-65,30	-19,14	26,29	4,96
'S061WTS014'	-63,25	-19,52	306,63	71,41
'S061WTS015'	-63,23	-19,79	328,94	76,57
'S061WTS017'	-63,54	-20,01	212,95	45,53
'S061WTS018'	-63,68	-19,93	506,86	117,86
'S061WTS019'	-63,87	-20,12	223,32	48,72
'S061WTS001'	-67,04	-15,16	696,35	186,63
'S061WTS020'	-63,94	-19,80	577,64	130,99
'S061WTS021'	-63,66	-19,17	385,15	88,53
'S061WTS022'	-63,66	-19,20	1585,68	472,99
'S061WTS002'	-67,11	-15,38	132,01	29,84
'S061WTS004'	-67,18	-15,51	90,21	21,05
'S061WTS005'	-67,43	-15,68	103,31	22,25
'S067WTS001'	-68,66	-24,24	0,95	0,23
'S067WTS002'	-69,17	-23,56	1,15	0,27
'S067WTS003'	-70,28	-24,08	0,82	0,21
'S067WTS004'	-69,47	-23,39	0,87	0,22
'S067WTS005'	-68,13	-23,79	1,89	0,42
'S067WTS007'	-69,46	-23,40	0,48	0,14
'S067WTS008'	-69,34	-23,58	0,30	0,11
'S074WTS001'	-76,90	-0,46	526,27	134,36
'S078WTS010'	-67,96	-17,12	4,30	0,83
'S078WTS011'	-67,86	-17,27	18,14	3,53
'S078WTS012'	-67,81	-17,29	26,09	4,82

'S078WTS013'	-67,64	-17,38	7,15	1,36
'S078WTS014'	-67,63	-17,39	5,06	0,98
'S078WTS015'	-67,62	-17,45	8,02	1,52
'S078WTS016'	-67,31	-17,28	12,50	2,34
'S078WTS017'	-67,40	-17,33	3,70	0,73
'S078WTS018'	-67,56	-17,37	7,81	1,48
'S078WTS019'	-68,05	-17,24	10,09	1,90
'S078WTS001'	-68,31	-16,64	12,41	2,35
'S078WTS002'	-68,31	-16,58	2,77	0,55
'S078WTS003'	-68,39	-16,54	5,60	1,06
'S078WTS005'	-68,27	-16,68	3,86	0,76
'S078WTS006'	-68,17	-16,91	7,72	1,46
'S078WTS007'	-68,19	-16,78	13,52	2,53
'S078WTS008'	-68,09	-17,05	4,85	0,94
'S078WTS009'	-67,99	-17,11	4,62	0,89
'S082WTS010'	-65,76	-24,73	70,55	12,85
'S082WTS011'	-65,73	-24,84	578,66	105,55
'S082WTS012'	-65,38	-24,61	872,19	173,31
'S082WTS015'	-65,92	-26,13	51,79	9,57
'S082WTS016'	-65,60	-24,72	142,47	26,78
'S082WTS017'	-64,88	-25,52	1090,47	269,36
'S082WTS018'	-66,00	-26,58	23,40	4,60
'S082WTS019'	-66,31	-25,43	81,81	14,83
'S082WTS001'	-65,62	-24,81	193,61	36,15
'S082WTS020'	-65,22	-22,80	127,85	23,25
'S082WTS021'	-66,12	-24,98	119,07	21,46
'S082WTS022'	-65,31	-22,93	3,42	0,67
'S082WTS023'	-66,27	-25,44	37,14	6,82
'S082WTS024'	-65,52	-25,43	371,87	71,91
'S082WTS025'	-65,79	-23,65	15,66	2,89
'S082WTS026'	-65,97	-25,79	124,47	23,14
'S082WTS027'	-65,96	-25,83	53,72	10,44
'S082WTS028'	-65,31	-24,17	27,80	5,09

'S082WTS029'	-65,49	-23,94	7658,08	2213,78
'S082WTS002'	-65,91	-27,32	706,30	128,98
'S082WTS030'	-65,36	-23,37	28,22	5,15
'S082WTS031'	-65,47	-23,74	42,06	7,68
'S082WTS032'	-65,55	-27,10	159,69	35,70
'S082WTS033'	-65,41	-27,02	178,18	36,60
'S082WTS034'	-66,09	-25,02	35,60	6,62
'S082WTS035'	-65,25	-26,24	127,10	26,19
'S082WTS036'	-65,70	-25,16	295,07	55,05
'S082WTS037'	-65,65	-25,16	603,96	119,03
'S082WTS038'	-65,33	-23,04	13,64	2,52
'S082WTS039'	-65,95	-26,58	61,96	11,35
'S082WTS003'	-64,81	-23,91	557,87	109,17
'S082WTS040'	-65,43	-24,71	298,79	58,13
'S082WTS041'	-65,39	-24,69	1055,47	197,99
'S082WTS004'	-64,82	-23,78	443,42	82,79
'S082WTS005'	-65,94	-27,40	73,90	14,27
'S082WTS006'	-65,86	-24,50	30,73	5,62
'S082WTS007'	-65,87	-24,54	14,57	2,69
'S082WTS008'	-65,87	-24,56	50,50	9,22
'S082WTS009'	-65,75	-24,76	840,62	154,00
'S094WTS010'	-71,41	-31,59	55,07	10,40
'S094WTS011'	-71,22	-31,66	47,20	8,98
'S094WTS012'	-71,33	-31,65	61,36	11,53
'S094WTS013'	-71,27	-31,69	66,75	12,49
'S094WTS014'	-70,54	-32,84	211,41	38,34
'S094WTS015'	-70,44	-33,58	257,22	46,99
'S094WTS016'	-70,53	-34,21	194,14	37,22
'S094WTS017'	-70,87	-34,68	163,23	30,24
'S094WTS018'	-70,88	-34,98	162,72	67,35
'S094WTS019'	-71,12	-35,19	175,07	53,33
'S094WTS001'	-69,99	-27,26	16,56	3,33
'S094WTS020'	-71,05	-35,72	101,59	19,81

'S094WTS002'	-70,77	-28,57	35,04	6,43
'S094WTS003'	-70,59	-28,68	37,74	6,88
'S094WTS004'	-70,46	-28,79	28,50	5,26
'S094WTS005'	-70,40	-28,79	51,65	9,36
'S094WTS006'	-70,50	-29,85	149,37	28,39
'S094WTS008'	-70,76	-30,34	35,76	6,62
'S094WTS009'	-71,12	-31,61	30,71	5,73
'S123WTS010'	-76,19	-13,03	68,33	13,45
'S123WTS012'	-76,36	-13,12	57,41	11,66
'S123WTS013'	-70,12	-17,85	47,82	14,28
'S123WTS014'	-70,18	-19,16	76,72	18,73
'S123WTS002'	-73,12	-15,93	71,38	15,79
'S123WTS004'	-73,63	-16,17	10,01	1,99
'S123WTS005'	-75,21	-14,52	40,66	7,88
'S123WTS007'	-75,93	-13,74	151,29	34,08
'S123WTS008'	-75,89	-12,80	62,55	11,84
'S123WTS009'	-75,94	-12,84	72,31	13,76
'S124WTS001'	-72,15	-37,59	64,42	17,26
'S124WTS002'	-72,01	-37,67	66,19	14,12
'S125WTS001'	-69,54	-33,28	287,79	57,28
'S125WTS002'	-69,46	-33,30	251,98	53,73
'S126WTS001'	-76,23	-13,08	59,90	11,56
'S127WTS010'	-65,96	-17,58	4,54	0,88
'S127WTS011'	-65,99	-17,56	7,61	1,47
'S127WTS012'	-66,38	-17,42	626,82	125,13
'S127WTS013'	-66,03	-17,87	136,03	25,97
'S127WTS014'	-66,35	-17,57	109,34	20,45
'S127WTS015'	-65,58	-18,21	115,51	22,57
'S127WTS016'	-66,39	-17,83	129,56	24,07
'S127WTS017'	-66,38	-17,83	69,97	12,93
'S127WTS018'	-66,42	-18,13	27,27	5,01
'S127WTS019'	-66,46	-18,22	37,03	6,82
'S127WTS001'	-65,11	-18,90	84,82	16,33

'S127WTS020'	-66,21	-18,46	22,93	4,22
'S127WTS021'	-66,32	-18,64	43,99	8,06
'S127WTS022'	-66,34	-18,64	67,41	12,47
'S127WTS023'	-66,28	-18,62	55,09	10,12
'S127WTS024'	-66,29	-18,63	51,43	9,41
'S127WTS025'	-66,16	-18,67	15,42	2,86
'S127WTS026'	-64,08	-19,61	69,49	13,79
'S127WTS027'	-64,08	-19,61	82,14	16,64
'S127WTS028'	-64,29	-19,16	16,44	3,21
'S127WTS029'	-64,32	-18,81	433,52	107,95
'S127WTS002'	-65,13	-18,92	38,34	7,71
'S127WTS030'	-64,31	-18,72	25,53	5,06
'S127WTS031'	-64,51	-18,69	58,72	11,74
'S127WTS032'	-64,73	-19,08	20,65	3,92
'S127WTS033'	-64,76	-19,05	14,80	2,81
'S127WTS034'	-65,00	-18,84	11,28	2,15
'S127WTS035'	-65,15	-18,60	51,57	10,10
'S127WTS036'	-64,44	-18,10	122,92	25,24
'S127WTS037'	-64,59	-18,09	40,11	7,96
'S127WTS038'	-64,77	-18,11	64,94	13,20
'S127WTS039'	-64,84	-18,14	36,65	7,31
'S127WTS003'	-65,13	-18,95	33,42	6,37
'S127WTS040'	-64,84	-18,13	17,88	3,42
'S127WTS004'	-65,19	-18,63	51,46	9,85
'S127WTS052'	-64,29	-18,56	29,70	5,77
'S127WTS057'	-65,58	-18,21	73,94	13,83
'S127WTS005'	-65,22	-17,92	25,25	4,82
'S127WTS006'	-65,29	-17,83	6,59	1,26
'S127WTS008'	-65,70	-18,35	329,82	63,76
'S127WTS009'	-65,86	-17,94	41,03	7,86
'S128WTS001'	-75,72	-13,61	53,21	-9999,99
'S128WTS002'	-75,65	-13,52	52,81	-9999,99
'S128WTS003'	-75,65	-13,51	47,92	-9999,99

'S128WTS004'	-75,68	-13,52	52,02	-9999,99
'S128WTS005'	-75,70	-13,57	48,18	-9999,99
'S128WTS006'	-75,71	-13,56	41,31	-9999,99
'S128WTS007'	-75,71	-13,57	49,33	-9999,99
'S129WTS001'	-65,76	-28,24	39,24	7,81
'S129WTS002'	-65,78	-28,19	35,92	6,97
'S129WTS003'	-65,93	-27,99	39,92	7,63
'S129WTS004'	-65,88	-28,22	110,95	21,26
'S129WTS005'	-65,91	-28,08	83,23	15,79
'S129WTS006'	-65,91	-28,08	48,57	9,17
'S130WTS010'	-65,52	-23,82	368,60	66,54
'S130WTS011'	-65,53	-23,81	72,72	13,17
'S130WTS014'	-65,34	-23,45	16,85	3,09
'S130WTS016'	-65,39	-23,59	29,57	5,40
'S130WTS018'	-65,37	-23,60	27,30	5,05
'S130WTS001'	-65,35	-23,38	65,52	11,89
'S130WTS020'	-65,37	-23,60	39,92	7,29
'S130WTS004'	-65,54	-23,66	36,54	6,68
'S130WTS007'	-65,57	-23,61	227,71	40,88
'S131WTS001'	-68,16	-31,37	50,08	10,01
'S131WTS003'	-67,87	-31,57	33,78	6,91
'S131WTS004'	-67,85	-31,07	85,40	16,78
'S135WTS010'	-73,39	5,06	58,31	11,32
'S135WTS011'	-73,40	5,23	14,86	2,87
'S135WTS012'	-73,37	5,15	51,68	9,97
'S135WTS013'	-73,39	5,30	46,78	9,05
'S135WTS014'	-73,96	4,78	17,13	3,29
'S135WTS015'	-73,82	4,97	3,40	0,68
'S135WTS016'	-74,08	4,96	7,48	1,45
'S135WTS017'	-73,41	5,45	4,77	0,94
'S135WTS018'	-73,57	5,66	6,99	1,38
'S135WTS019'	-73,60	5,92	9,14	1,79
'S135WTS001'	-73,91	4,59	75,83	14,54

'S135WTS020'	-73,25	6,51	45,78	8,99
'S135WTS022'	-73,27	6,67	63,33	12,51
'S135WTS002'	-73,90	4,45	71,17	14,17
'S135WTS003'	-73,91	4,38	69,06	13,47
'S135WTS004'	-73,69	4,03	470,41	114,40
'S135WTS005'	-73,82	4,21	650,52	138,40
'S135WTS006'	-73,83	4,26	98,23	19,97
'S135WTS007'	-73,91	4,40	76,06	14,84
'S135WTS008'	-74,12	4,49	14,30	2,70
'S135WTS009'	-73,73	5,09	10,64	2,05
'S161WTS011'	-78,39	-2,72	113,64	23,52
'S161WTS013'	-78,43	-2,75	128,09	25,61
'S161WTS014'	-78,56	-2,53	196,79	39,68
'S161WTS018'	-78,46	-2,60	250,73	54,01
'S161WTS019'	-78,92	-2,97	54,94	11,15
'S161WTS001'	-78,93	-2,94	37,48	7,60
'S161WTS020'	-78,90	-2,96	19,55	3,77
'S161WTS023'	-78,91	-2,94	43,21	8,74
'S161WTS028'	-78,77	-2,90	43,15	8,66
'S161WTS002'	-78,70	-3,25	62,01	12,49
'S161WTS033'	-78,80	-3,14	22,76	4,48
'S161WTS034'	-78,81	-3,14	60,25	12,76
'S161WTS036'	-78,56	-3,00	85,89	16,99
'S161WTS039'	-78,60	-3,01	15,93	3,09
'S161WTS003'	-78,89	-2,91	67,03	14,12
'S161WTS004'	-78,93	-2,77	72,72	14,23
'S161WTS005'	-78,89	-2,88	36,28	7,31
'S161WTS008'	-78,93	-3,03	21,23	4,10
'S161WTS009'	-78,92	-2,70	96,38	20,20
'S173WTS001'	-65,53	-23,94	13839,88	3462,19
'S173WTS003'	-65,52	-23,94	467,94	86,44
'S173WTS007'	-65,49	-23,94	1779,19	334,55
'S178WST001'	-70,40	-28,79	51,03	9,34

'S178WST003'	-70,46	-28,79	28,34	5,48
'S178WST005'	-70,59	-28,68	37,68	6,93
'S178WST007'	-70,77	-28,57	35,03	6,55
'S188WTS010'	-74,26	-15,85	14,74	2,86
'S188WTS011'	-74,52	-15,67	21,03	3,98
'S188WTS012'	-74,64	-15,63	66,10	12,50
'S188WTS013'	-75,25	-14,66	45,53	8,63
'S188WTS014'	-75,68	-14,35	28,54	5,49
'S188WTS015'	-76,13	-13,46	85,81	15,97
'S188WTS016'	-76,24	-13,32	25,25	4,92
'S188WTS017'	-76,40	-13,13	66,29	12,35
'S188WTS018'	-76,64	-12,67	62,88	11,71
'S188WTS019'	-76,74	-12,50	26,39	5,33
'S188WTS001'	-70,33	-18,09	13,00	2,47
'S188WTS020'	-76,89	-12,25	39,00	7,37
'S188WTS021'	-77,24	-11,61	97,38	18,37
'S188WTS022'	-77,59	-11,07	136,68	25,58
'S188WTS023'	-77,70	-10,85	43,38	8,26
'S188WTS024'	-77,83	-10,65	33,64	6,46
'S188WTS026'	-78,81	-8,43	14,91	2,95
'S188WTS027'	-79,01	-8,14	22,96	4,47
'S188WTS028'	-79,48	-7,32	30,29	5,92
'S188WTS029'	-79,66	-7,00	13,57	2,89
'S188WTS002'	-70,51	-17,83	28,54	5,33
'S188WTS030'	-79,85	-6,45	22,60	4,64
'S188WTS031'	-79,61	-6,79	32,19	6,47
'S188WTS032'	-79,18	-7,83	52,30	10,41
'S188WTS033'	-78,43	-9,25	64,94	12,37
'S188WTS034'	-78,30	-9,48	54,01	10,28
'S188WTS035'	-78,27	-9,49	59,77	11,46
'S188WTS036'	-78,22	-9,94	35,61	7,16
'S188WTS037'	-78,15	-10,07	20,40	3,90
'S188WTS038'	-76,99	-11,79	82,33	15,53

	'S188WTS039'	-77,77	-10,72	267,37	50,41
	'S188WTS003'	-70,96	-17,90	14,98	2,83
	'S188WTS040'	-76,62	-11,92	199,65	44,03
	'S188WTS041'	-69,96	-18,58	20,12	3,75
	'S188WTS042'	-69,62	-19,41	34,18	6,29
	'S188WTS004'	-70,99	-17,29	20,43	3,81
	'S188WTS009'	-73,62	-16,23	8,53	1,69
o	'S025WTS010'	-68,48	-15,34	305,07	72,34
o	'S025WTS035'	-67,22	-16,78	129,84	24,99
o	'S025WTS009'	-68,49	-15,35	77,80	16,32
o	'S035WTS014'	-78,81	-2,99	2,81	0,58
o	'S035WTS015'	-78,80	-2,95	18,47	3,64
o	'S035WTS001'	-78,90	-2,96	17,36	3,42
o	'S059WTS015'	-79,95	-4,93	122,62	35,06
o	'S059WTS016'	-79,95	-4,92	140,08	29,23
o	'S059WTS017'	-80,01	-4,98	68,24	16,26
o	'S059WTS018'	-80,02	-4,99	131,53	34,78
o	'S059WTS001'	-79,89	-4,91	5,63	1,10
o	'S059WTS020'	-80,07	-5,04	47,48	12,72
o	'S059WTS021'	-79,81	-5,03	43,04	8,79
o	'S059WTS024'	-79,88	-5,10	26,96	6,02
o	'S059WTS025'	-79,89	-5,12	19,31	4,45
o	'S061WTS011'	-64,15	-19,54	29,82	5,94
o	'S061WTS007'	-63,26	-19,79	234,76	57,32
o	'S061WTS008'	-64,03	-19,79	685,84	145,37
o	'S067WTS006'	-70,06	-24,09	0,41	0,15
o	'S085WTS001'	-69,03	-32,34	10,27	1,98
o	'S085WTS002'	-69,14	-32,55	8,32	1,58
o	'S085WTS003'	-69,15	-32,58	6,30	1,24
o	'S085WTS004'	-69,10	-32,65	106,13	20,38
o	'S085WTS005'	-68,98	-32,37	53,74	11,69
o	'S085WTS006'	-68,96	-32,50	85,81	17,57
o	'S131WTS002'	-67,87	-31,06	91,15	23,91

o	'S161WTS010'	-78,90	-2,67	151,29	33,97
o	'S161WTS012'	-78,39	-2,73	152,80	32,74
o	'S161WTS015'	-78,61	-2,65	155,74	31,75
o	'S161WTS016'	-78,46	-2,66	149,44	30,54
o	'S161WTS017'	-78,57	-2,61	148,18	31,31
o	'S161WTS024'	-78,80	-2,94	19,13	3,73
o	'S161WTS031'	-78,69	-2,98	83,58	15,85
o	'S161WTS032'	-78,81	-3,16	7,31	1,45
o	'S161WTS035'	-78,81	-3,00	2,49	0,52
o	'S173WTS010'	-65,51	-23,95	70,15	13,14
o	'S173WTS005'	-65,53	-23,94	607,68	112,00
*	Val et al 2018	-68,72	-29,91	104,00	8,67
*	Val et al 2018	-69,01	-30,34	117,00	7,60
*	Val et al 2018	-69,67	-30,29	24,70	0,49
*	Val et al 2018	-69,04	-31,20	67,00	2,08
*	Val et al 2018	-69,88	-31,35	52,00	1,21
*	Val et al 2018	-69,95	-32,34	223,00	33,80
*	Val et al 2018	-69,97	-33,80	262,00	10,80
*	Val et al 2018	-69,72	-34,47	98,50	3,85

o Computed using the 30 m resolution SRTM dataset (see main text for references and details)

* Not yet added to octopus database. Rates recalculated to Stone (2000) scalling scheme, same as Octopus database.

Stone, J. O.: Air pressure and cosmogenic isotope production, J. Geophys. Res.-Sol. Ea., 105, 23753–23759, https://doi.org/10.1029/2000JB900181, 2000. a, b

Val, P., Venerdini, A. L., Ouimet, W., Alvarado, P., & Hoke, G. D. (2018). Tectonic control of erosion in the southern Central Andes. Earth and Planetary Science Letters, 482, 160-170, https://doi.org/10.1016/j.epsl.2017.11.004

Topographic Data (extracted using Topographic Analysis Kit)						
drainage_area'	'mean_ksn	'se_ksn'	'mean_gra	'se_gradient'	'mean_pre	'se_precip'
(km^2)	(m)	(m)	(m/m)	(m/m)	(mm/a)	(mm/a)
3227,70	525,32	7,85	0,46	0,00	858,55	1,11
432,21	440,32	14,91	0,52	0,00	1750,49	4,41
5836,26	504,75	5,65	0,48	0,00	1133,38	1,15
227,31	267,26	12,02	0,47	0,00	3260,46	3,67
252,81	276,36	11,90	0,46	0,00	3167,31	3,76
1537,84	497,97	14,00	0,50	0,00	1311,33	2,97
1762,40	449,63	12,47	0,51	0,00	2085,39	3,46
5356,09	324,95	5,32	0,44	0,00	2204,58	1,17
134,51	496,31	30,72	0,43	0,00	255,82	0,70
1454,05	460,69	12,03	0,55	0,00	2513,97	3,22
25,90	256,01	108,57	0,29	0,00	3045,76	1,39
155,25	239,78	22,34	0,44	0,00	2929,77	1,72
148,03	356,09	23,75	0,55	0,00	2868,39	1,45
40,68	293,79	23,13	0,45	0,00	2147,17	3,09
160,81	526,82	48,59	0,54	0,00	828,28	2,66
167,15	543,60	38,79	0,55	0,00	695,84	2,33
38,00	574,04	58,71	0,52	0,00	1069,44	5,29
447,97	636,39	28,91	0,56	0,00	870,83	2,30
124,23	216,54	24,77	0,27	0,00	401,91	0,65
41,54	504,22	60,19	0,46	0,00	642,36	1,46
1355,83	333,31	8,09	0,38	0,00	480,72	0,41
46,47	324,21	20,16	0,42	0,00	1241,80	2,04
210,37	483,16	21,69	0,51	0,00	724,58	3,13
26,29	400,60	19,64	0,58	0,00	1462,95	3,80
16,92	504,74	102,39	0,46	0,00	631,87	1,06
1098,02	496,87	16,08	0,54	0,00	1014,25	2,11
6255,33	420,96	5,74	0,42	0,00	560,78	0,41
69,89	329,95	18,85	0,45	0,00	1657,34	2,67

153,69	476,43	25,26	0,52	0,00	1278,36	3,81
1459,04	533,20	12,35	0,56	0,00	1151,33	1,66
417,51	418,40	14,24	0,49	0,00	1575,41	1,87
638,81	619,08	20,87	0,59	0,00	810,99	2,07
31,78	542,02	50,46	0,51	0,00	656,75	1,00
350,19	588,42	23,91	0,62	0,00	767,45	2,50
24,64	785,76	128,22	0,60	0,01	551,31	5,18
63,11	419,78	40,82	0,57	0,00	356,60	0,57
76,45	538,26	50,41	0,65	0,00	326,59	0,68
32,10	569,00	77,91	0,46	0,00	691,81	2,75
2983,63	535,04	7,86	0,45	0,00	692,62	0,64
199,01	636,18	40,07	0,51	0,00	488,08	1,91
27,38	611,06	61,02	0,57	0,00	1269,03	3,73
272,95	107,27	4,31	0,23	0,00	1070,51	0,56
24,24	150,12	13,15	0,18	0,00	1105,62	0,77
39,09	186,61	10,49	0,20	0,00	1304,77	2,31
21,43	123,34	16,36	0,21	0,00	1117,89	0,59
30,54	128,34	16,89	0,21	0,00	1083,33	1,00
50,86	74,69	5,58	0,24	0,00	1115,12	1,86
140,43	95,05	4,37	0,24	0,00	1100,16	0,82
18,52	104,51	10,61	0,27	0,00	1098,70	0,63
2552,24	252,98	9,69	0,21	0,00	129,93	0,12
3028,74	266,36	8,80	0,22	0,00	117,26	0,12
3342,70	269,91	8,24	0,21	0,00	108,64	0,11
882,54	127,10	4,10	0,15	0,00	139,99	0,18
1630,10	148,38	4,15	0,15	0,00	128,67	0,13
147,61	401,65	20,66	0,38	0,00	663,98	1,36
2944,56	260,53	5,31	0,35	0,00	537,53	0,27
5496,39	169,74	3,50	0,24	0,00	490,86	0,20
6440,31	152,39	3,11	0,22	0,00	470,07	0,19
7728,57	128,65	2,64	0,19	0,00	433,71	0,18
11,55	298,65	26,27	0,43	0,00	552,12	1,59
44,09	351,21	30,39	0,34	0,00	878,57	1,14

104,83	331,12	17,15	0,36	0,00	636,87	0,85
155,58	345,60	16,63	0,38	0,00	619,68	0,78
184,76	311,16	15,68	0,35	0,00	581,85	0,87
194,84	299,80	16,38	0,34	0,00	572,81	0,86
13,39	454,80	39,74	0,48	0,00	667,30	0,80
26,96	353,01	33,86	0,40	0,00	607,28	1,25
51,35	361,05	24,86	0,38	0,00	617,75	0,90
137,36	388,06	22,20	0,37	0,00	683,96	1,34
3932,28	199,32	3,20	0,32	0,00	981,34	0,37
1331,95	171,08	5,12	0,28	0,00	683,71	0,41
129,69	68,54	4,99	0,24	0,00	783,48	0,84
152,53	80,43	3,44	0,26	0,00	526,66	0,40
5193,80	105,64	1,82	0,27	0,00	837,64	0,27
21,99	109,35	10,31	0,37	0,00	732,37	0,90
1066,58	81,82	2,23	0,24	0,00	841,81	0,31
48,86	141,42	13,14	0,26	0,00	1469,03	1,33
52,09	89,03	11,00	0,29	0,00	763,29	0,49
3125,80	75,92	1,71	0,21	0,00	690,37	0,31
49,73	97,15	11,88	0,27	0,00	866,09	1,38
333,36	120,27	5,80	0,26	0,00	1765,60	1,11
207,83	138,73	6,09	0,25	0,00	1453,08	1,40
35,46	201,87	13,32	0,36	0,00	1989,66	2,36
21,56	136,36	20,03	0,16	0,00	25,95	0,33
4413,41	86,75	9,54	0,08	0,00	10,82	0,02
551,00	137,42	5,75	0,14	0,00	10,26	0,02
761,27	83,69	2,43	0,06	0,00	19,33	0,04
335,02	160,30	8,57	0,11	0,00	100,20	0,33
761,59	81,56	2,35	0,06	0,00	19,73	0,04
5196,82	96,05	16,29	0,07	0,00	11,29	0,02
8284,66	207,52	3,57	0,25	0,00	2705,58	1,33
27,27	72,65	5,53	0,13	0,00	412,98	0,58
51,56	137,35	15,00	0,21	0,00	257,06	0,59
31,78	130,79	6,81	0,27	0,00	206,21	0,37

33,22	109,84	9,47	0,16	0,00	259,51	0,52
103,96	99,11	4,88	0,15	0,00	231,10	0,26
300,06	53,90	2,73	0,09	0,00	389,48	0,41
113,83	69,03	4,05	0,13	0,00	308,59	0,49
87,44	36,24	3,10	0,08	0,00	363,83	0,32
176,60	73,37	3,49	0,12	0,00	360,36	0,51
334,00	63,91	2,41	0,09	0,00	422,40	0,44
335,88	57,40	4,01	0,08	0,00	542,15	0,43
117,67	94,51	9,87	0,17	0,00	530,72	0,74
1436,88	35,59	1,31	0,06	0,00	520,36	0,29
14,72	9,42	1,20	0,02	0,00	428,33	1,95
17,75	28,95	1,95	0,06	0,00	438,43	0,87
65,01	45,14	3,17	0,09	0,00	373,95	0,63
184,63	28,65	1,98	0,07	0,00	459,32	0,41
38,53	82,56	6,50	0,14	0,00	505,18	0,77
188,03	337,00	21,14	0,32	0,00	157,91	0,73
1010,24	384,48	8,81	0,42	0,00	215,46	0,21
172,44	212,24	13,58	0,30	0,00	626,63	0,55
7674,71	173,85	2,51	0,19	0,00	351,23	0,15
154,00	358,89	14,20	0,40	0,00	257,45	1,38
167,44	153,70	10,52	0,23	0,00	1134,00	1,40
24,56	41,28	5,24	0,05	0,00	381,61	1,18
1388,02	326,39	10,52	0,31	0,00	204,64	0,34
68,04	439,86	26,11	0,47	0,00	349,38	1,79
126,57	344,34	17,90	0,37	0,00	242,91	0,36
1499,68	339,72	6,68	0,36	0,00	193,46	0,11
146,66	119,42	7,17	0,20	0,00	282,36	0,59
1563,11	234,62	7,54	0,27	0,00	241,58	0,35
326,96	226,91	8,16	0,37	0,00	611,81	1,16
17,34	99,08	8,35	0,13	0,00	122,43	0,13
277,01	242,67	12,74	0,27	0,00	353,86	0,63
28,26	79,06	7,98	0,12	0,00	686,40	2,14
6184,75	256,33	4,12	0,29	0,00	310,03	0,24

22,40	395,91	32,38	0,54	0,00	281,54	0,69
206,00	554,31	27,95	0,47	0,00	535,39	1,68
945,72	162,99	5,61	0,23	0,00	246,32	0,22
4432,41	207,98	3,35	0,25	0,00	296,89	0,19
35,35	119,64	14,41	0,24	0,00	999,95	1,25
104,04	197,25	16,73	0,28	0,00	790,73	1,12
314,27	176,33	8,47	0,21	0,00	194,49	0,36
1815,40	109,24	3,37	0,18	0,00	872,48	0,48
330,82	293,56	14,11	0,37	0,00	195,69	0,59
362,76	295,59	13,34	0,38	0,00	232,77	0,80
996,27	120,63	3,51	0,19	0,00	302,19	0,22
289,38	306,16	18,46	0,23	0,00	261,82	0,29
1402,45	243,57	6,70	0,32	0,00	770,39	0,55
130,01	235,56	13,98	0,34	0,00	805,06	1,17
642,10	309,25	12,79	0,34	0,00	495,08	1,00
2194,85	387,72	7,64	0,44	0,00	515,76	0,50
731,60	145,30	6,80	0,20	0,00	505,93	0,51
1665,99	184,31	4,75	0,25	0,00	188,65	0,12
507,59	233,74	9,66	0,28	0,00	191,27	0,14
136,58	229,10	10,40	0,22	0,00	159,77	0,53
2923,41	224,66	4,32	0,27	0,00	184,43	0,10
6004,20	322,82	4,43	0,36	0,00	186,43	0,09
1991,17	320,18	7,86	0,36	0,00	178,52	0,11
5935,96	323,37	4,51	0,36	0,00	184,16	0,09
3757,47	335,95	5,91	0,37	0,00	177,78	0,10
2123,23	480,74	9,66	0,51	0,00	331,27	0,35
4943,16	454,11	6,09	0,50	0,00	489,51	0,26
2161,54	443,01	8,45	0,53	0,00	714,19	0,43
1466,00	451,50	9,06	0,48	0,00	979,69	0,77
1241,10	366,95	7,65	0,46	0,00	1071,38	0,89
1791,44	288,05	8,14	0,34	0,00	663,21	0,57
3963,11	250,65	4,63	0,26	0,00	33,03	0,03
2712,08	308,41	6,92	0,37	0,00	444,20	0,57

7948,06	422,91	4,83	0,41	0,00	51,07	0,03
7344,19	443,35	5,01	0,43	0,00	54,07	0,03
2929,43	439,63	7,06	0,44	0,00	52,02	0,04
3922,34	454,32	7,12	0,42	0,00	60,76	0,04
2922,28	481,62	8,64	0,46	0,00	86,68	0,08
1171,15	420,74	11,10	0,44	0,00	81,05	0,06
1230,82	409,41	12,02	0,40	0,00	162,56	0,12
5726,88	485,55	8,90	0,43	0,00	344,62	0,22
6016,27	473,33	8,45	0,42	0,00	328,99	0,22
537,05	411,89	16,61	0,36	0,00	111,43	0,16
2211,31	238,89	6,76	0,21	0,00	26,96	0,08
1065,43	302,27	12,36	0,27	0,00	70,20	0,14
1347,43	252,27	10,09	0,22	0,00	20,73	0,09
1860,48	407,11	13,57	0,33	0,00	257,05	0,23
3697,46	415,39	9,95	0,24	0,00	249,16	0,25
3679,47	465,97	11,18	0,43	0,00	419,24	0,23
971,95	559,85	24,70	0,43	0,00	379,39	0,51
1093,53	140,20	4,65	0,23	0,00	NaN	NaN
7615,77	194,04	2,36	0,30	0,00	NaN	NaN
263,75	458,45	19,90	0,52	0,00	100,35	0,59
309,78	461,93	18,58	0,51	0,00	101,09	0,50
5840,29	480,21	8,58	0,43	0,00	338,41	0,22
557,47	86,66	3,70	0,17	0,00	741,63	0,40
634,02	85,91	3,61	0,16	0,00	759,35	0,40
146,39	340,73	21,33	0,36	0,00	512,48	1,37
5525,78	154,51	2,48	0,23	0,00	721,46	0,29
987,71	241,44	5,15	0,33	0,00	556,76	0,55
9901,01	191,15	2,24	0,27	0,00	707,33	0,25
1136,62	225,85	6,95	0,31	0,00	419,52	0,36
666,38	192,16	7,61	0,29	0,00	478,54	0,52
504,76	93,07	5,07	0,15	0,00	376,95	0,41
511,39	132,88	9,98	0,19	0,00	425,70	0,59
253,13	179,65	7,72	0,32	0,00	768,60	0,77

2920,97	142,02	3,90	0,21	0,00	394,31	0,26
967,56	160,20	4,86	0,27	0,00	403,26	0,44
117,61	136,22	8,55	0,29	0,00	395,21	0,68
1102,67	158,77	4,56	0,28	0,00	405,22	0,40
1323,91	139,53	4,71	0,21	0,00	368,47	0,26
609,07	132,04	4,20	0,22	0,00	424,76	0,42
950,00	165,29	6,69	0,28	0,00	927,32	0,40
3868,67	201,20	3,16	0,32	0,00	985,24	0,37
246,42	120,55	7,13	0,26	0,00	814,28	0,87
25,39	442,32	50,65	0,50	0,00	489,08	1,00
322,49	178,00	8,42	0,29	0,00	746,85	0,98
860,75	215,59	7,49	0,33	0,00	586,66	0,48
1715,14	174,44	5,60	0,27	0,00	713,59	0,50
243,69	112,34	4,13	0,28	0,00	752,25	0,71
251,66	142,30	7,14	0,29	0,00	574,54	0,39
333,75	162,59	7,89	0,25	0,00	636,76	0,28
509,34	173,75	5,09	0,31	0,00	875,61	0,60
530,26	114,90	4,52	0,22	0,00	355,37	0,26
627,20	191,16	5,00	0,30	0,00	344,41	0,39
139,20	143,29	11,19	0,27	0,00	326,58	0,40
467,00	115,67	3,83	0,23	0,00	681,67	0,78
1147,97	152,43	3,23	0,30	0,00	1010,36	0,61
5367,54	156,91	2,40	0,26	0,00	695,03	0,28
2072,09	176,74	3,09	0,31	0,00	930,30	0,46
9809,37	176,99	1,94	0,27	0,00	581,22	0,21
9901,01	191,15	2,24	0,27	0,00	707,33	0,25
2667,36	166,65	3,28	0,27	0,00	804,55	0,36
1130,87	178,43	6,95	0,26	0,00	588,49	0,58
1679,66	266,43	4,92	0,37	0,00	937,16	0,69
188,86	211,34	9,66	0,32	0,00	779,70	0,52
300,00	341,37	15,94	0,39	0,00	70,30	0,17
74,67	301,51	31,55	0,35	0,00	86,75	0,16
57,57	347,50	29,67	0,41	0,00	66,31	0,15

38,69	273,93	29,60	0,41	0,00	123,09	0,41
205,16	333,09	19,88	0,38	0,00	84,08	0,18
50,64	277,09	18,85	0,42	0,00	47,04	0,35
258,25	323,97	16,61	0,39	0,00	76,37	0,18
1341,91	234,98	6,18	0,26	0,00	824,34	0,53
992,08	208,17	6,49	0,23	0,00	781,13	0,64
309,74	207,72	9,47	0,24	0,00	719,73	0,85
140,61	432,95	22,85	0,44	0,00	940,03	0,95
109,47	342,84	22,56	0,31	0,00	611,65	1,87
51,15	271,34	20,02	0,25	0,00	698,82	2,80
102,55	385,34	38,02	0,36	0,00	162,31	0,58
86,21	371,39	44,76	0,35	0,00	166,74	0,68
184,01	311,40	25,91	0,33	0,00	130,64	0,32
112,50	357,73	31,94	0,30	0,00	82,79	0,13
84,58	305,82	33,71	0,29	0,00	84,43	0,12
948,74	163,11	5,60	0,23	0,00	246,23	0,22
40,77	342,87	24,89	0,34	0,00	79,30	0,27
49,40	245,02	18,91	0,35	0,00	125,43	0,78
19,21	306,26	18,13	0,38	0,00	72,89	0,21
82,71	302,87	17,05	0,37	0,00	329,05	0,41
16,14	183,68	23,79	0,26	0,00	347,90	0,59
13,97	389,47	55,25	0,43	0,00	645,34	2,10
1405,99	257,42	6,61	0,23	0,00	1079,82	0,50
390,95	236,71	11,07	0,23	0,00	951,37	0,74
1190,25	242,67	6,99	0,23	0,00	1075,90	0,57
484,45	196,63	7,74	0,18	0,00	1051,17	0,84
162,91	134,26	7,37	0,19	0,00	873,98	1,00
308,39	102,30	5,98	0,16	0,00	834,83	0,80
132,26	129,61	12,13	0,18	0,00	985,86	1,01
111,51	97,25	10,22	0,15	0,00	774,32	0,43
414,82	145,66	7,36	0,18	0,00	1466,16	1,00
1186,39	165,60	5,74	0,20	0,00	1393,20	1,14
240,25	346,12	17,02	0,28	0,00	1349,54	1,36

2329,67	277,34	6,72	0,31	0,00	2759,07	2,09
9905,11	216,69	3,82	0,24	0,00	2337,76	1,00
616,26	364,76	10,99	0,28	0,00	1439,71	1,05
911,06	343,91	8,49	0,28	0,00	1422,33	0,85
2954,30	392,12	6,61	0,35	0,00	1386,56	2,21
1010,25	449,75	14,10	0,39	0,00	1171,39	2,77
1391,55	366,51	7,72	0,31	0,00	1505,65	1,14
293,15	347,08	18,79	0,25	0,00	1083,23	1,83
242,08	210,75	9,55	0,18	0,00	478,49	1,24
277,30	90,24	5,44	0,16	0,00	981,91	0,78
725,63	443,46	17,92	0,47	0,00	2199,70	2,10
668,74	440,20	19,34	0,47	0,00	2136,39	2,09
424,76	380,00	23,01	0,36	0,00	722,79	1,98
15,50	502,65	30,94	0,58	0,00	2266,89	8,53
18,73	104,57	10,95	0,27	0,00	1097,98	0,63
140,60	96,79	4,90	0,24	0,00	1100,00	0,82
21,92	126,33	19,72	0,21	0,00	1116,28	0,61
30,93	126,10	15,70	0,21	0,00	1081,35	1,01
79,36	261,83	35,98	0,34	0,00	1072,65	1,56
121,70	374,26	17,11	0,47	0,00	1575,02	1,26
22,60	178,11	27,89	0,28	0,00	1265,39	3,53
54,91	141,94	20,07	0,17	0,00	1042,46	1,85
105,67	313,48	17,70	0,46	0,00	1513,23	5,76
27,65	345,80	34,92	0,45	0,00	1128,10	5,25
24,48	148,50	13,35	0,18	0,00	1105,43	0,76
40,27	184,53	11,47	0,20	0,00	1296,36	2,36
272,79	106,90	4,41	0,23	0,00	1070,50	0,56
58,30	75,61	4,84	0,24	0,00	1117,26	1,65
58,91	249,70	18,13	0,27	0,00	1040,02	2,71
10,70	357,95	64,85	0,61	0,01	263,87	0,76
18,68	387,92	43,57	0,57	0,00	284,76	0,71
21,86	389,05	36,06	0,55	0,00	280,88	0,68
3921,94	452,87	7,13	0,42	0,00	60,76	0,04

2929,41	439,95	7,12	0,44	0,00	52,01	0,04
7344,19	443,68	5,03	0,43	0,00	54,07	0,03
7951,18	423,16	4,92	0,41	0,00	51,06	0,03
1232,50	387,89	10,39	0,34	0,00	39,14	0,13
4315,21	354,63	7,39	0,29	0,00	220,75	0,28
4512,32	341,62	7,87	0,26	0,00	289,96	0,32
5221,78	374,22	6,79	0,32	0,00	215,93	0,15
4635,21	258,95	5,26	0,27	0,00	116,14	0,13
3090,36	473,17	10,49	0,38	0,00	184,60	0,20
619,47	391,49	14,40	0,33	0,00	55,69	0,18
6034,38	466,02	8,30	0,42	0,00	328,01	0,22
2320,13	509,17	12,29	0,42	0,00	291,72	0,30
709,62	343,93	12,06	0,36	0,00	154,22	0,31
917,57	335,89	11,70	0,29	0,00	86,10	0,17
1562,89	418,29	11,90	0,38	0,00	175,90	0,24
2893,32	430,11	10,20	0,40	0,00	253,79	0,25
4279,46	454,06	7,78	0,44	0,00	304,32	0,25
983,12	411,26	14,23	0,39	0,00	186,28	0,38
2348,72	411,84	8,15	0,40	0,00	217,42	0,27
1724,00	340,56	12,12	0,31	0,00	294,12	0,49
2097,67	335,96	10,64	0,33	0,00	577,39	0,70
3869,00	373,53	7,53	0,35	0,00	690,75	0,44
1756,68	218,35	9,33	0,25	0,00	704,35	1,14
2107,66	331,65	8,44	0,30	0,00	104,33	0,13
1367,48	254,97	10,17	0,29	0,00	523,62	0,71
3526,16	297,08	6,53	0,30	0,00	814,18	0,62
4236,75	353,28	4,73	0,40	0,00	617,20	0,50
1707,06	406,02	10,82	0,40	0,00	235,71	0,37
744,07	364,46	15,22	0,38	0,00	221,78	0,50
1797,39	460,50	12,51	0,41	0,00	304,92	0,39
677,74	367,04	13,76	0,38	0,00	231,08	0,80
2089,04	388,90	10,31	0,37	0,00	208,60	0,28
1754,76	435,75	11,73	0,40	0,00	279,41	0,32

4418,92	516,89	8,92	0,46	0,00	417,42	0,33
4192,91	235,44	4,71	0,20	0,00	43,88	0,07
1189,50	551,16	17,87	0,49	0,00	328,47	0,34
1413,34	303,61	11,26	0,25	0,00	83,80	0,14
649,30	230,08	15,45	0,21	0,00	75,93	0,14
1776,64	322,05	9,29	0,26	0,00	110,61	0,15
1392,14	252,13	9,68	0,23	0,00	20,21	0,08
4,68	363,51	37,12	0,52	0,01	2690,09	2,80
3,73	381,06	23,89	0,64	0,01	1745,87	8,51
1,51	293,95	0,00	0,47	0,01	2442,45	3,72
8,53	232,55	39,80	0,30	0,00	1102,52	0,93
2,62	207,15	7,67	0,31	0,01	1064,18	0,80
1,33	81,33	0,00	0,15	0,00	1036,12	1,21
8,28	281,45	39,22	0,46	0,01	779,21	3,10
4,59	247,69	25,05	0,41	0,01	706,47	2,08
3,29	239,13	53,47	0,46	0,01	698,87	1,03
1,43	278,50	0,00	0,39	0,01	634,67	1,08
1,02	4,40	0,00	0,10	0,01	786,42	2,40
1,77	103,80	12,81	0,29	0,01	380,80	0,41
4,75	193,61	37,07	0,39	0,01	688,58	0,97
7,43	243,03	42,28	0,41	0,01	409,98	1,01
3,56	280,06	23,00	0,57	0,01	372,19	0,60
8,27	281,92	44,42	0,48	0,01	919,41	1,39
4,20	84,77	24,75	0,54	0,01	525,02	0,84
4,90	157,39	23,56	0,41	0,01	646,23	0,95
8,74	77,83	7,60	0,16	0,00	11,18	0,14
1,68	71,48	0,00	0,11	0,00	36,29	0,04
1,51	125,49	0,00	0,15	0,00	114,52	0,12
2,25	69,05	0,00	0,12	0,00	107,07	0,18
4,54	152,53	27,83	0,34	0,01	149,43	0,40
4,56	75,17	7,99	0,26	0,01	59,23	0,34
5,77	134,72	14,05	0,31	0,00	459,16	1,45
2,34	241,77	0,00	0,55	0,01	722,49	1,59

5,46	161,05	11,64	0,21	0,00	1178,46	3,58
9,58	423,44	58,53	0,53	0,01	2689,36	3,75
7,39	387,16	48,82	0,43	0,00	1383,09	2,21
8,96	456,14	46,52	0,57	0,00	2020,10	6,74
3,74	371,91	43,45	0,47	0,01	1737,17	1,79
7,74	305,39	25,39	0,31	0,00	1075,35	0,82
2,24	187,82	32,24	0,36	0,01	1178,95	2,63
0,68	123,94	0,00	0,32	0,02	1168,26	3,35
8,45	212,79	35,39	0,30	0,00	1102,07	0,93
1,80	319,52	0,00	0,56	0,01	361,96	2,03
7,65	395,09	55,74	0,53	0,01	315,45	0,43
135,32	127,63	6,76	0,25	0,00	107,58	0,68
140,92	211,02	13,99	0,22	0,00	99,09	0,38
1017,11	398,48	10,21	0,39	0,00	178,51	0,24
166,69	282,82	15,93	0,31	0,00	141,59	0,50
1373,59	415,07	11,20	0,43	0,00	193,61	0,23
4853,14	333,97	4,45	0,41	0,00	183,38	0,10
2475,72	430,74	7,90	0,46	0,00	209,25	0,17
2806,41	283,76	5,52	0,34	0,00	150,96	0,15

Data Table S3: Excluded erosion rate data.

Octopus Erosion Rate Dataset				
Octopus Flag	**X_WGS84**	**Y_WGS84**	**EBE_MMKYR**	**EBE_ERR**
	°Lon	°Lat	(or m/Ma)	1s
'S025WTS016'	-67,86	-15,50	132,42	25,53
'S025WTS047'	-67,17	-16,16	362,02	70,47
'S025WTS056'	-67,53	-14,01	511,91	101,33
'S059WTS026'	-80,59	-6,02	-9999,99	-9999,99
'S074WTS010'	-76,97	-0,47	392,36	129,07
'S074WTS011'	-73,44	-2,94	366,50	166,09
'S074WTS012'	-73,02	-3,37	103,03	32,88
'S074WTS013'	-76,69	-0,46	632,90	299,32
'S074WTS014'	-76,30	-0,48	455,87	189,46
'S074WTS015'	-76,14	-0,45	771,87	426,95
'S074WTS016'	-74,09	-2,36	57,24	21,53
'S074WTS002'	-75,71	-0,67	590,11	483,78
'S074WTS003'	-75,54	-0,79	580,69	548,39
'S074WTS004'	-75,47	-0,87	613,84	342,52
'S074WTS005'	-75,14	-1,02	566,74	378,74
'S074WTS006'	-75,14	-1,02	391,77	240,72
'S074WTS007'	-74,64	-1,87	391,47	192,83
'S074WTS008'	-74,01	-2,41	195,06	119,58
'S074WTS009'	-73,71	-2,46	335,42	148,03
'S078WTS020'	-68,13	-17,46	51,43	9,52
'S078WTS004'	-68,27	-16,72	-9999,99	-9999,99
'S082WTS013'	-65,15	-25,12	492,00	91,13
'S082WTS014'	-65,75	-25,95	82,99	15,21
'S091WTS001'	-72,78	-49,48	107,10	21,46
'S123WTS001'	-73,13	-15,92	273,74	69,49
'S123WTS003'	-73,16	-16,19	247,60	48,24
'S126WTS002'	-73,14	-16,35	208,12	46,26
'S127WTS041'	-63,56	-19,09	502,85	140,07

'S127WTS042'	-63,56	-18,86	705,18	201,05
'S127WTS043'	-63,67	-19,10	428,08	106,55
'S127WTS044'	-63,69	-19,02	416,59	96,29
'S127WTS045'	-63,67	-19,40	748,45	256,01
'S127WTS046'	-63,67	-19,18	234,70	57,76
'S127WTS047'	-63,68	-19,40	537,64	143,29
'S127WTS048'	-63,81	-19,68	260,66	61,50
'S127WTS049'	-64,04	-19,66	576,73	147,86
'S127WTS050'	-63,32	-18,83	102,23	19,73
'S127WTS051'	-64,11	-18,97	74,57	14,44
'S127WTS053'	-64,37	-18,62	72,56	13,78
'S127WTS054'	-64,89	-18,50	106,33	19,99
'S127WTS055'	-65,19	-18,62	123,67	23,04
'S127WTS056'	-65,37	-18,43	170,81	32,32
'S127WTS007'	-65,37	-18,43	147,88	27,55
'S135WTS021'	-73,40	-7,10	164,89	37,32
'S135WTS023'	-73,40	-7,10	222,34	42,91
'S188WTS025'	-78,62	-8,97	69,01	13,01
'S188WTS005'	-71,75	-17,10	89,81	16,66
'S188WTS006'	-72,74	-16,61	127,78	23,41
'S188WTS007'	-72,42	-16,72	33,89	6,38
'S188WTS008'	-73,11	-16,43	242,31	45,33
'S078WTS004'	-69,27	-16,73	-9999,99	-9999,99
Val et al 2018	-69,37	-29,02	32,40	0,66
'S025WTS011'	-68,28	-15,30	185,72	34,89
'S025WTS033'	-67,21	-16,77	420,86	83,39
'S025WTS034'	-67,21	-16,77	287,20	55,44
'S025WTS040'	-67,22	-16,76	164,78	31,87
'S025WTS043'	-67,30	-16,48	370,90	69,11
'S025WTS052'	-67,81	-16,36	323,53	61,99
'S025WTS053'	-67,81	-16,36	204,10	38,35
'S035WTS011'	-78,89	-2,88	33,98	6,58
'S048WTS006'	-69,88	-18,35	24,01	6,21

'S048WTS007'	-70,30	-18,40	23,74	4,54
'S048WTS008'	-69,88	-18,35	19,64	3,98
'S061WTS016'	-63,23	-19,79	320,69	90,69
'S061WTS003'	-67,11	-15,38	138,54	30,92
'S061WTS006'	-67,43	-15,68	205,16	44,86
'S061WTS009'	-64,08	-19,61	75,22	14,62
'S094WTS007'	-70,50	-29,85	141,43	26,18
'S123WTS011'	-76,19	-13,03	70,49	16,64
'S123WTS006'	-75,21	-14,52	18,84	3,74
'S130WTS012'	-65,53	-23,81	201,61	36,40
'S130WTS013'	-65,53	-23,81	518,75	93,52
'S130WTS015'	-65,34	-23,45	19,09	3,50
'S130WTS017'	-65,39	-23,59	55,38	10,08
'S130WTS019'	-65,37	-23,60	14,18	2,63
'S130WTS021'	-65,37	-23,60	74,05	13,47
'S130WTS002'	-65,35	-23,38	44,50	8,10
'S130WTS003'	-65,35	-23,38	21,82	3,99
'S130WTS005'	-65,54	-23,66	60,51	11,03
'S130WTS006'	-65,54	-23,66	49,73	9,07
'S130WTS008'	-65,57	-23,61	321,45	57,89
'S130WTS009'	-65,52	-23,82	72,06	13,06
'S161WTS029'	-78,77	-2,90	55,71	10,90
'S161WTS030'	-78,77	-2,90	54,75	11,10
'S161WTS037'	-78,56	-3,00	85,25	17,05
'S161WTS038'	-78,56	-3,00	88,55	17,36
'S161WTS006'	-78,89	-2,88	34,00	6,60
'S173WTS002'	-65,53	-23,94	118864,46	56403,27
'S173WTS004'	-65,52	-23,94	657,86	121,69
'S173WTS008'	-65,49	-23,94	2618,88	493,04
'S178WST002'	-70,40	-28,79	73,94	13,93
'S178WST004'	-70,46	-28,79	74,72	14,90
'S178WST006'	-70,59	-28,68	103,83	20,87
'S178WST008'	-70,77	-28,57	84,99	15,99

'S025WTS036'	-67,22	-16,78	118,25	23,04
'S025WTS037'	-67,22	-16,78	135,23	26,26
'S025WTS038'	-67,22	-16,78	137,38	26,63
'S035WTS016'	-78,80	-2,95	21,51	4,33
'S035WTS017'	-78,80	-2,95	22,46	4,42
'S035WTS002'	-78,90	-2,96	19,88	3,86
'S061WTS012'	-64,15	-19,54	34,94	7,96
'S078WTS013'	-67,64	-17,35	7,15	1,36
'S078WTS001'	-68,30	-16,64	12,41	2,35
'S078WTS002'	-68,31	-16,58	2,77	0,55
'S078WTS003'	-68,39	-16,55	5,50	1,06
'S078WTS005'	-68,27	-16,68	3,86	0,76
'S082WTS001'	-65,62	-24,81	193,61	36,15
'S082WTS002'	-65,91	-27,32	706,30	128,98
'S082WTS032'	-65,56	-27,10	159,69	35,70
'S135WTS014'	-73,91	4,56	17,13	3,29
'S135WTS001'	-73,91	4,59	75,83	14,54
'S135WTS002'	-73,90	4,45	71,17	14,17
'S135WTS003'	-73,91	4,38	69,06	13,47
'S161WTS025'	-78,80	-2,94	22,25	4,50
'S161WTS026'	-78,80	-2,94	23,27	4,60
'S173WTS006'	-65,53	-23,94	384,43	70,82
'S173WTS009'	-65,51	-23,95	188,49	35,26

Topographic Data (extracted using Topographic Analysis Kit)							
drainage_area'	'mean_ksn	'se_ksn'	'mean_gra	'se_gradie	'mean_pre	'se_precip'	
(km^2)	(m)	(m)	(m/m)	(m/m)	(mm/a)	(mm/a)	obs
13635,83	368,15	3,68	0,43	0,00	1600,15	0,88	area > 1e4
10980,68	441,99	4,00	0,47	0,00	978,64	0,59	area > 1e4
70496,09	322,79	3,48	0,38	0,00	1403,16	0,29	area > 1e4
50,96	4,99	1,30	0,01	0,00	23,62	0,10	no erosion rate
11427,58	178,42	2,89	0,22	0,00	3199,10	1,17	area > 1e4
89597,10	62,16	0,71	0,09	0,00	2655,91	0,25	area > 1e4
99916,16	56,72	0,63	0,09	0,00	2644,66	0,22	area > 1e4
18813,81	193,16	2,36	0,23	0,00	2950,30	0,93	area > 1e4
20477,49	177,83	2,21	0,22	0,00	2937,71	0,85	area > 1e4
20677,44	176,14	2,19	0,22	0,00	2933,76	0,85	area > 1e4
26457,40	17,43	0,31	0,05	0,00	2541,00	0,19	area > 1e4
22272,28	163,71	2,09	0,20	0,00	2890,08	0,80	area > 1e4
22677,89	160,83	2,06	0,20	0,00	2874,54	0,78	area > 1e4
27182,59	135,64	1,75	0,17	0,00	2848,11	0,66	area > 1e4
44279,35	112,02	1,26	0,15	0,00	2800,34	0,47	area > 1e4
44279,35	112,02	1,26	0,15	0,00	2800,34	0,47	area > 1e4
50046,17	100,31	1,16	0,14	0,00	2758,82	0,42	area > 1e4
79346,48	68,64	0,75	0,10	0,00	2672,37	0,27	area > 1e4
84857,60	65,29	0,73	0,10	0,00	2659,48	0,26	area > 1e4
23988,15	55,58	0,54	0,10	0,00	334,97	0,07	area > 1e4
105,95	25,13	1,56	0,03	0,00	466,88	0,85	no erosion rate
33642,38	206,53	1,45	0,25	0,00	360,90	0,12	area > 1e4
14886,09	214,80	2,16	0,25	0,00	261,01	0,11	area > 1e4
1237,61	215,87	6,66	0,38	0,00	NaN	NaN	area > 1e4
14021,30	370,49	5,87	0,28	0,00	369,56	0,13	area > 1e4
15585,87	367,83	5,41	0,28	0,00	337,26	0,14	area > 1e4
15819,97	363,75	5,27	0,28	0,00	332,99	0,14	area > 1e4
647,55	56,17	5,47	0,17	0,00	676,05	0,48	soft sed. Rock

1209,58	138,07	4,56	0,28	0,00	1172,93	0,64	soft sed. Rock
3208,74	76,90	1,73	0,21	0,00	694,51	0,30	soft sed. Rock
1014,35	175,41	6,12	0,33	0,00	1040,17	0,63	soft sed. Rock
900,60	45,90	1,57	0,13	0,00	724,19	0,37	soft sed. Rock
2486,06	82,99	1,96	0,23	0,00	678,24	0,37	soft sed. Rock
563,45	62,34	2,98	0,21	0,00	601,62	0,46	soft sed. Rock
164,47	77,27	5,23	0,26	0,00	592,24	1,01	soft sed. Rock
42,73	82,11	6,21	0,38	0,00	726,04	1,59	soft sed. Rock
59648,69	192,00	1,01	0,29	0,00	733,91	0,12	area > 1e4
43809,00	203,43	1,20	0,29	0,00	672,90	0,13	area > 1e4
32266,75	207,64	1,46	0,30	0,00	701,60	0,16	area > 1e4
26634,27	208,27	1,59	0,30	0,00	719,80	0,19	area > 1e4
22479,57	208,60	1,73	0,29	0,00	692,70	0,21	area > 1e4
11402,63	218,15	2,69	0,30	0,00	638,65	0,33	area > 1e4
11402,63	218,15	2,69	0,30	0,00	638,65	0,33	area > 1e4
21112,45	273,45	2,80	0,28	0,00	1836,61	0,63	area > 1e4
14804,47	307,71	3,29	0,31	0,00	1775,77	0,78	area > 1e4
11932,51	410,99	4,79	0,39	0,00	542,63	0,26	area > 1e4
12975,67	282,46	4,39	0,25	0,00	205,57	0,11	area > 1e4
17108,51	283,30	5,00	0,24	0,00	245,76	0,12	area > 1e4
13312,48	189,25	3,98	0,16	0,00	136,08	0,10	area > 1e4
15962,35	364,60	5,27	0,28	0,00	329,65	0,14	area > 1e4
97,12	20,48	1,33	0,03	0,00	474,99	0,92	no erosion rate
15073,56	223,78	2,44	0,24	0,00	109,98	0,05	area > 1e4
3227,70	525,32	7,85	0,46	0,00	858,55	1,11	replicate
210,37	483,16	21,69	0,51	0,00	724,58	3,13	replicate
210,37	483,16	21,69	0,51	0,00	724,58	3,13	replicate
26,29	400,60	19,64	0,58	0,00	1462,95	3,80	replicate
6255,33	420,96	5,74	0,42	0,00	560,78	0,41	replicate
24,64	785,76	128,22	0,60	0,01	551,31	5,18	replicate
24,64	785,76	128,22	0,60	0,01	551,31	5,18	replicate
272,95	107,27	4,31	0,23	0,00	1070,51	0,56	replicate
2552,24	252,98	9,66	0,21	0,00	129,93	0,12	replicate

3342,70	269,91	8,24	0,21	0,00	108,64	0,11	replicate
2552,24	252,98	9,66	0,21	0,00	129,93	0,12	replicate
152,53	80,43	3,44	0,26	0,00	526,66	0,40	replicate
333,36	120,27	5,80	0,26	0,00	1765,60	1,11	replicate
35,46	201,87	13,92	0,36	0,00	1989,66	2,36	replicate
3932,28	199,32	3,20	0,32	0,00	981,34	0,37	replicate
2922,28	481,62	8,64	0,46	0,00	66,68	0,08	replicate
5726,88	485,55	8,90	0,43	0,00	344,62	0,22	replicate
1860,48	407,11	13,57	0,33	0,00	257,05	0,23	replicate
86,21	371,39	44,76	0,35	0,00	166,74	0,68	replicate
86,21	371,39	44,76	0,35	0,00	166,74	0,68	replicate
184,01	311,40	25,91	0,33	0,00	130,64	0,32	replicate
112,50	357,73	31,94	0,30	0,00	82,79	0,13	replicate
84,58	305,82	33,71	0,29	0,00	84,43	0,12	replicate
40,77	342,87	24,89	0,34	0,00	79,30	0,27	replicate
948,74	163,11	5,60	0,23	0,00	246,23	0,22	replicate
948,74	163,11	5,60	0,23	0,00	246,23	0,22	replicate
49,40	245,02	18,91	0,35	0,00	125,43	0,78	replicate
49,40	245,02	18,91	0,35	0,00	125,43	0,78	replicate
19,21	306,26	18,13	0,38	0,00	72,89	0,21	replicate
102,55	385,34	38,02	0,36	0,00	162,31	0,58	replicate
79,36	261,83	35,98	0,34	0,00	1072,65	1,56	replicate
79,36	261,83	35,98	0,34	0,00	1072,65	1,56	replicate
105,67	313,48	17,70	0,46	0,00	1513,23	5,76	replicate
105,67	313,48	17,70	0,46	0,00	1513,23	5,76	replicate
272,79	106,90	4,41	0,23	0,00	1070,50	0,56	replicate
10,70	357,95	64,85	0,61	0,01	263,87	0,76	replicate
18,68	387,92	43,57	0,57	0,00	284,76	0,71	replicate
21,86	389,05	36,06	0,55	0,00	280,88	0,68	replicate
3921,94	452,87	7,13	0,42	0,00	60,76	0,04	replicate
2929,41	439,95	7,12	0,44	0,00	52,01	0,04	replicate
7344,19	443,68	5,03	0,43	0,00	54,07	0,03	replicate
7951,18	423,16	4,92	0,41	0,00	51,06	0,03	replicate

3,73	381,06	23,89	0,64	0,01	1745,87	8,51	replicate
3,73	381,06	23,89	0,64	0,01	1745,87	8,51	replicate
3,73	381,06	23,89	0,64	0,01	1745,87	8,51	replicate
2,62	207,15	7,67	0,31	0,01	1064,18	0,80	replicate
2,62	207,15	7,67	0,31	0,01	1064,18	0,80	replicate
1,33	81,33	0,00	0,15	0,00	1056,12	1,21	replicate
8,27	281,92	44,42	0,48	0,01	919,41	1,39	replicate
31,45	98,34	6,59	0,20	0,00	226,12	0,28	replicate
163,37	38,26	2,72	0,04	0,00	549,60	0,62	replicate
256,94	60,68	3,84	0,10	0,00	553,18	0,53	replicate
1454,69	30,62	0,94	0,07	0,00	520,39	0,29	replicate
8,55	10,04	0,96	0,02	0,00	435,10	2,97	replicate
66,89	394,53	19,25	0,49	0,00	346,75	1,79	replicate
205,82	479,10	22,55	0,48	0,00	534,94	1,68	replicate
36,25	120,15	11,57	0,25	0,00	995,40	1,28	replicate
170,87	265,87	14,37	0,31	0,00	1318,81	0,89	replicate
240,72	281,05	12,94	0,28	0,00	1349,88	1,36	replicate
615,49	291,31	8,16	0,29	0,00	1439,96	1,05	replicate
913,09	287,41	6,70	0,29	0,00	1422,50	0,85	replicate
7,74	305,39	25,39	0,31	0,00	1075,35	0,82	replicate
7,74	305,39	25,39	0,31	0,00	1075,35	0,82	replicate
7,65	395,09	55,74	0,53	0,01	315,45	0,43	replicate
1,80	319,52	0,00	0,56	0,01	361,96	2,03	replicate